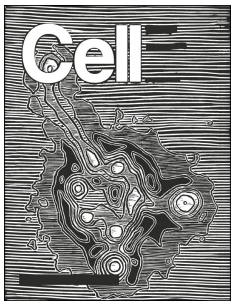

Case Study: Prolonged infectious SARS-CoV-2 shedding from an asymptomatic immunocompromised cancer patient.

Victoria A. Avanzato, M. Jeremiah Matson, Stephanie N. Seifert, Rhys Pryce, Brandi N. Williamson, Sarah L. Anzick, Kent Barbian, Seth D. Judson, Elizabeth R. Fischer, Craig Martens, Thomas A. Bowden, Emmie de Wit, Francis X. Riedo, Vincent J. Munster

PII: S0092-8674(20)31456-2

DOI: https://doi.org/10.1016/j.cell.2020.10.049

Reference: CELL 11714

To appear in: *Cell*

Received Date: 20 September 2020

Revised Date: 13 October 2020

Accepted Date: 28 October 2020

Please cite this article as: Avanzato, V.A., Matson, M.J., Seifert, S.N., Pryce, R., Williamson, B.N., Anzick, S.L., Barbian, K., Judson, S.D., Fischer, E.R., Martens, C., Bowden, T.A., de Wit, E., Riedo, F.X., Munster, V.J., Case Study: Prolonged infectious SARS-CoV-2 shedding from an asymptomatic immunocompromised cancer patient., *Cell* (2020), doi: https://doi.org/10.1016/j.cell.2020.10.049.

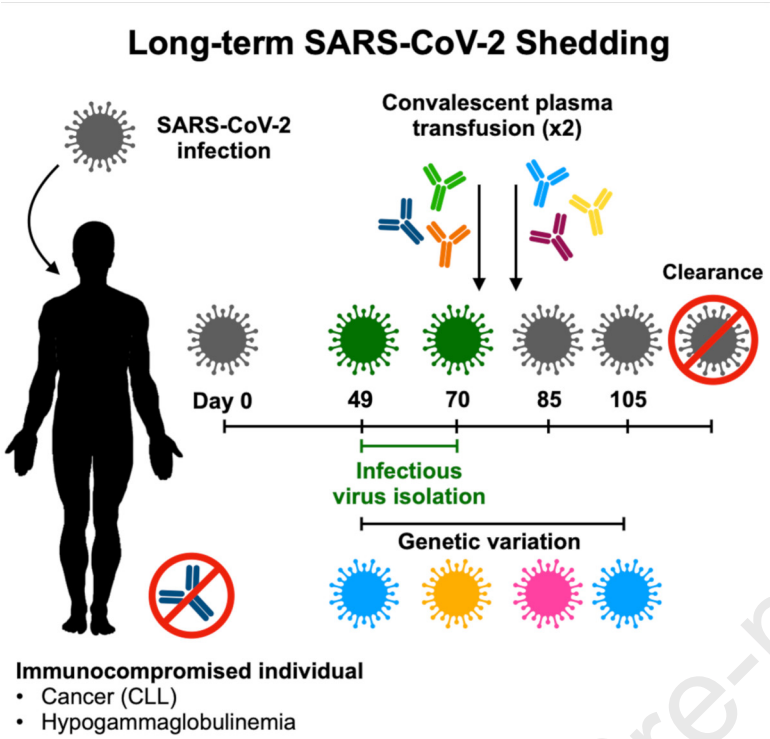

Case Study: Prolonged infectious SARS-CoV-2 shedding from an asymptomatic immunocompromised cancer patient.

Victoria A. Avanzato[1,2,7], M. Jeremiah Matson[1,3,7], Stephanie N. Seifert[1,7], Rhys Pryce[2], Brandi N. Williamson[1], Sarah L. Anzick[4], Kent Barbian[4], Seth D. Judson[5], Elizabeth R. Fischer[4], Craig Martens[4], Thomas A. Bowden[2], Emmie de Wit[1], Francis X. Riedo[6,8*], Vincent J. Munster[1,8,9*].

1. *Laboratory of Virology, National Institute of Allergy and Infectious Diseases, National Institutes of Health, Hamilton, MT 59840, USA*
2. *Division of Structural Biology, Wellcome Centre for Human Genetics, University of Oxford, Oxford OX3 7BN, UK*
3. *Marshall University Joan C. Edwards School of Medicine, Huntington, WV 25701, USA*
4. *Research Technologies Branch, National Institute of Allergy and Infectious Diseases, National Institutes of Health, Hamilton, MT 59840, USA*
5. *Department of Medicine, University of Washington, Seattle, WA 98195, USA*
6. *EvergreenHealth, Kirkland, WA 98034, USA*
7. *These authors contributed equally.*
8. *Joint corresponding authors.*
9. *Lead contact*

**Correspondence: vincent.munster@nih.gov, FXRiedo@evergreenhealthcare.org*

Summary

Long-term SARS-CoV-2 shedding was observed from the upper respiratory tract of a female immunocompromised patient with chronic lymphocytic leukemia and acquired hypogammaglobulinemia. Shedding of infectious SARS-CoV-2 was observed up to 70 days, and genomic and subgenomic RNA up to 105 days past initial diagnosis. The infection was not cleared after a first treatment with convalescent plasma, suggesting limited impact on SARS-CoV-2 in the upper respiratory tract within this patient. Several weeks after a second convalescent plasma transfusion, SARS-CoV-2 RNA was no longer detected. We observed marked within-host genomic evolution of SARS-CoV-2, with continuous turnover of dominant viral variants. However, replication kinetics in Vero E6 cells and primary human alveolar epithelial tissues were not affected. Our data indicate that certain immunocompromised patients may shed infectious virus for longer durations than previously recognized. Detection of subgenomic RNA is recommended in persistently SARS-CoV-2 positive individuals as a proxy for shedding of infectious virus.

Introduction

SARS-CoV-2 RNA can be detected from various sites, including samples obtained from the nares, nasopharynx, pharynx, bronchoalveolar lavage (BAL) fluid, feces, and blood (Wang et al., 2020, Sun et al., 2020, Judson and Munster, 2020). The duration of SARS-CoV-2 RNA shedding is generally between 3 and 46 days after symptom onset (Fu et al., 2020, Qian et al., 2020, Liu et al., 2020c). Asymptomatic patients shed SARS-CoV-2 RNA comparably with symptomatic cases in regards to duration and viral loads (Lee et al., 2020, Long et al., 2020, Zou et al., 2020). Persistent SARS-CoV-2 RNA shedding has been documented with patients remaining qRT-PCR positive for up to 63 days (Li et al., 2020, Liu et al., 2020b). In addition, there are reports of patients testing positive again after a period of negative testing in both symptomatic and asymptomatic cases (Lan et al., 2020, Hu et al., 2020). As qRT-PCR detects viral RNA but does not confirm the presence of infectious SARS-CoV-2, these observations raise questions about the duration of infectious SARS-CoV-2 shedding and transmission potential in both symptomatic and asymptomatic cases.

Estimates suggest that infectiousness begins 2.3 days prior to symptom onset and declines within 7 days of symptom onset (He et al., 2020b). Consistent with this, infectious SARS-CoV-2 has been isolated from patient samples taken up to 8 days after symptom onset, but typically not thereafter (Wolfel et al., 2020, Bullard et al., 2020). In contrast to the prolonged shedding of SARS-CoV-2 RNA, the longest detected shedding of infectious SARS-CoV-2 virus is up to 20 days after the initial positive test result (van Kampen et al., 2020, Liu et al., 2020b). The probability of isolating SARS-CoV-2 decreases with lower viral load, when the duration of symptoms exceeds 15 days, and upon the generation of detectable neutralizing antibodies (van Kampen et al., 2020).

On January 19, 2020 the first case of coronavirus disease 2019 (COVID-19) was identified in the United States of America (USA) in Snohomish County, Washington, in a traveller returning from Wuhan, China. Community spread in the Seattle region became evident in late February of 2020 (Bhatraju et al., 2020), with extensive spread in a long-term care facility (McMichael et al., 2020a). Here, we describe an asymptomatic, immunocompromised patient persistently testing positive for SARS-CoV-2 by qRT-PCR who was infected during the early phase of SARS-CoV-2 spread in the USA. Infectious SARS-CoV-2 was successfully isolated from nasopharyngeal swabs 49 days and 70 days past the initial positive qRT-PCR test. Convalescent plasma treatment was not immediately successful in clearing the infection, but evidence of SARS-CoV-2 RNA was eventually cleared after 105 days.

Results

Clinical presentation of an immunocompromised patient persistently infected with SARS-CoV-2

On February 12, 2020, a 71-year-old woman with a 10-year history of chronic lymphocytic leukemia (CLL), acquired hypogammaglobulinemia, anemia, and chronic leukocytosis presented to the emergency department with low back and lower extremity pain. She underwent surgery for a spinal fracture and stenosis related to her cancer on February 14, 2020 (biopsy results in Table S1) and was subsequently transferred to a rehabilitation facility on February 19, 2020. On February 25, 2020, she was re-hospitalized for anemia and underwent a chest X-ray the following day, which was normal. She could not return to her rehabilitation center due to a confirmed outbreak of COVID-19 at the facility (McMichael et al., 2020a, McMichael et al., 2020b). A chest CT performed on February 28, 2020, was unremarkable. The patient had no respiratory or systemic symptoms during this time. Because she was residing in the rehabilitation facility around the time

of the COVID-19 outbreak, she was tested and found positive for SARS-CoV-2 on March 2, 2020 (Figure 1). After the initial SARS-CoV-2 diagnosis, the patient was kept in isolation at an isolation ward in a single room with negative airflow. Attending medical staff were using full personal protective equipment comprised of Powered Air Purifying Respirators (PAPR) or N95 respirators with goggles, gowns and gloves. Over the course of the next 15 weeks, she was tested for SARS-CoV-2 another 14 times by several diagnostic companies and remained positive on testing through June 15, 2020, 105 days since the initial positive test. Subsequently, the patient tested negative on four consecutive swabs from June 16 to July 16, indicating her infection had cleared.

Due to acquired hypogammaglobulinemia caused by her CLL, the patient received intravenous immunoglobulin (IVIG) every 4 to 6 weeks as part of her treatment regimen. She received IVIG treatment on both April 6 and May 6, 2020. The manufacture date of her specific lot of IVIG preceded January 1, 2020, before the beginning of the COVID-19 pandemic and therefore did not contribute to any SARS-CoV-2 serology results (Table S2). Due to the persistence of her SARS-CoV-2 infection, serum samples were tested for antibodies against the spike glycoprotein through a study at the NIH Clinical Center and no spike-specific antibodies were detected (Burbelo et al., 2020). On May 12, 2020, she was transfused with 200 mL of SARS-CoV-2 convalescent plasma provided by Bloodworks Northwest under an FDA eIND protocol with a virus neutralizing (VN) titer of 60 (Table 1). Her infection persisted, and on May 23, 2020, she received another 200 mL dose of convalescent plasma from a different donor with a VN titer of 160 under the same protocol (Table 1). Additional laboratory values are available in Table S3.

Long-term shedding of genomic RNA, subgenomic RNA and infectious SARS-CoV-2

SARS-CoV-2 shedding kinetics within the patient were monitored using the detection of genomic RNA (gRNA), subgenomic RNA (sgRNA) and infectious SARS-CoV-2. RNA was extracted from nasopharyngeal and oropharyngeal swabs collected at 49, 70, 77, 85, 105, and 136 days from the initial diagnosis and evaluated for the presence of viral gRNA (Corman et al., 2020) and sgRNA (Wolfel et al., 2020). gRNA and sgRNA were detected in nasopharyngeal swabs out to day 105, except for the swab taken at day 77 (Figure 2A), though the test through EvergreenHealth was positive at this time. None of the oropharyngeal swabs were positive, for gRNA or sgRNA, suggesting the infection was confined to the nasopharynx. Absolute quantification of gRNA and sgRNA on positive swabs was performed by droplet digital PCR (ddPCR) (Figure 2A). The highest viral load was detected in the day 70 swab, at 2.2×10^6 gRNA copies/mL (CT 22.44), and 1.1×10^5 sgRNA copies/mL (CT 29.05). The detection of sgRNA in swabs is indicative of active SARS-CoV-2 replication, as only actively replicating SARS-CoV-2 would initiate RNA synthesis resulting in replication and transcription of sgRNAs (Wang Y., 2020, Kim et al., 2020) and sgRNA, unlike gRNA, does not persist in the nasal cavity in the absence of virus replication (Speranza et al., 2020). Virus isolation was attempted on all qRT-PCR positive samples. Infectious SARS-CoV-2 was successfully cultured from the nasopharyngeal swabs collected at day 49 and day 70. Scanning and transmission electron microscopy on SARS-CoV-2 cultured from the nasopharyngeal swabs collected on day 49 and 70 shows viral particles consistent with coronavirus morphology, supporting a persistent SARS-CoV-2 infection with shedding of infectious virus in this patient (Figure 3).

Convalescent plasma treatment did not clear SARS-CoV-2 from the upper respiratory tract

In an attempt to treat the persistent SARS-CoV-2 infection, the patient received two doses of convalescent plasma therapy on day 71 and 82. Pre- and post-transfusion serum samples and the transfusion convalescent plasma samples were analyzed for the presence of full-length spike and spike receptor binding domain (RBD) antibodies by ELISA assay and of SARS-CoV-2 neutralizing antibodies in a virus neutralization (VN) assay (Figure 2B and 2C, Figure S1A and S1B, and Table 1) (Amanat et al., 2020, Wrapp et al., 2020). The first dose of convalescent plasma (convalescent plasma 1) had an IgG spike titer of 2560, RBD titer of 3840 and a VN titer of 60. The second dose of convalescent plasma (convalescent plasma 2) had an IgG spike titer of 5120, RBD titer of 5120 and a VN titer of 160 (Figure 2B, S1A, Table 1). Prior to the first dose of plasma given on day 71, detectable spike and RBD IgG antibody titers were very low in serum collected from the patient, with IgG titers between 1:10 and 1:40 at day 49 and 71 pre transfusion; no VN titers were detected in these samples. Immediately after the first transfusion at day 71, the spike and RBD IgG antibody titers rose to 1:320 and then decreased to 1:80 and 1:160 respectively at day 77. No VN titers were detected at day 71 and 77 (Figure 2C, S1B, Table 1). Immediately after the second transfusion at day 82 the spike and RBD IgG titers increased to 1:320 and 1:640 respectively and remained elevated by day 105 (Figure 2C, S1B). Low neutralizing titers of 1:10 were observed at day 82 and 105 (Table 1).

Despite two transfusions of convalescent plasma, nasopharyngeal swabs at day 85 and 105 remained positive for both gRNA and sgRNA, suggesting that the convalescent plasma therapy was not successful in rapidly clearing the infection from the upper respiratory tract in this patient. Although the presence of sgRNA at these timepoints suggests active viral replication, infectious SARS-CoV-2 could not be cultured after day 70.

Genetic analysis of patient swab samples links infection to the primary Washington State outbreak

SARS-CoV-2 full genome sequences were obtained from nasopharyngeal swabs collected at days 49, 70, 85, and 105 (Table S4). Full genomes were obtained by sequencing using the ARTIC primer set (https://artic/network/) and assembling reads to MN985325.1 (USA/WA1/2020) as the reference genome (Harcourt et al., 2020). The SARS-CoV-2 lineage was determined using Pangolin software (https://pangolin.cog-uk.io/), which placed the patient viral genomes in lineage A.1, which consists of genomes originating from the primary outbreak in Washington state (Rambaut et al., 2020). A maximum-likelihood tree was generated using representative SARS-CoV-2 genomes from previously described lineages (Rambaut et al., 2020) obtained from the GISAID database (www.gisaid.org) (Shu and McCauley, 2017). The patient SARS-CoV-2 full length genomes cluster together within lineage A.1 (Figure 4A). This suggests that the patient was infected with a virus from the SARS-CoV-2 A.1 lineage, which circulated after the initial import from China, followed by exponential growth and local transmission in Washington state.

In order to visualize the temporal relationships of the patient isolates, forty-four full SARS-CoV-2 genome sequences from Washington state belonging to NextStrain clade 19B (clades.nextstrain.org) were subsampled from the GISAID database (www.gisaid.org) (Shu and McCauley, 2017) representing strains collected in Washington state from February to May, 2020. A full genome alignment was performed with four of the full genome sequences recovered from the persistently infected patient, the USA/WA1/2020 genome sequence, and the Wuhan-Hu-1/2019 genome sequence with MAFFT v. 1.4 (Katoh and Standley, 2013, Katoh et al., 2002) implemented in Geneious Prime v. 2020.1.2 (www.geneious.com). A maximum likelihood tree was reconstructed with PhyML v. 3.1 (Guindon et al., 2010) and a tree showing temporal

184 divergence (Figure 4B) was inferred in TreeTime v. 0.7.6 (Sagulenko et al., 2018, Hadfield et al.,
185 2018) using the HKY85 model of nucleotide substitution and a fixed molecular clock at 8e-4 with
186 a standard deviation of 4e-4 as implemented in the NextStrain pipeline (nextstrain.org/sars-cov-2/).
187 Divergence dating estimates place the patient isolates sharing a most recent common ancestor
188 between February 27th and March 31st, 2020, within 90% of the marginal probability distribution.
189 This is consistent with the timing of patient's first positive test on March 2, 2020. To further
190 evaluate the relationship between the SARS-CoV-2 genomes recovered from the patient swabs
191 with other SARS-CoV-2 genomes circulating in Washington state at the times of sampling (April
192 20, May 11, May 26, and June 15, 2020), Washington SARS-CoV-2 genomes were downloaded
193 from the GISAID database (Shu and McCauley, 2017). Quality of the sequences was determined
194 by the Nextclade server v.0.7.5 (https://clades/nextstrain.org/) and 1,789 sequences at April 20,
195 385 sequences between April 20 and May 11, 268 sequences between May 11 and May 26, and
196 709 sequences between May 26 and June 15, were kept for further phylogenetic analysis.
197 Maximum likelihood trees using the curated sets of sequences, the four patient genomes, and the
198 USA/WA1/2020 genome were inferred using ModelFinder (Kalyaanamoorthy et al., 2017) and
199 ultrafast bootstrap (Hoang et al., 2018) implemented in IQ-TREE v1.6.12 (Nguyen et al., 2015).
200 The phylogenetic trees show that the patient genomes in this study cluster as a monophyletic clade
201 consistent with infection in late February/early March followed by viral persistence (Figure S2).
202
203 Next, full genome sequences from the two SARS-CoV-2 isolates were obtained (Table S4), and
204 the consensus level variants in the sequences obtained from nasopharyngeal swabs and SARS-
205 CoV-2 isolates cultured from those swabs were compared to the reference strain USA/WA1/2020
206 (MN985325.1) (Harcourt et al., 2020). Several single nucleotide (nt) substitutions were observed

within ORF1ab, spike, M and ORF8 coding sequence in the full genome sequences obtained directly from the patient swabs and the SARS-CoV-2 isolates. In addition, a 3 nt deletion leading to the loss of a methionine residue was observed in nsp1 in day 49 and day 70 samples (Table 2). Within the genomes of the two SARS-CoV-2 isolates, two in-frame deletions were observed in the spike glycoprotein coding region. A 21 nt in-frame deletion (residue 21,975 – 21,995) was found in the N-terminal domain (NTD) of S1, leading to a 7 amino acid deletion (aa 139-145) within the spike glycoprotein of the SARS-CoV-2 day 49 isolate. A smaller 12 nt deletion (residues 21,982 – 21,993) was detected in the day 70 isolate, leading to a 4 amino acid deletion (aa 141-144) in the NTD, which falls within the 7-amino acid deletion found in the day 49 isolate (Figure 5A). These observed deletions in the spike glycoprotein map to a region in the NTD that is partially solvent-exposed and forms a β-strand in a compact conformation of the spike (Wrobel et al., 2020) (Figure 5B and 5C). This region is unmodelled in other structures representing additional conformational states of the spike, and thus is likely flexible (Wrapp et al., 2020, Walls et al., 2020). It is possible that the apparent plasticity within this region of the molecule may contribute to the structural permissibility of the identified deletions. The position of these deletions is distinct from those observed in other SARS-CoV-2 isolates, which locate to the S1/S2 and S2' cleavage sites (Andres et al., 2020, Lau et al., 2020, Liu et al., 2020d).

Comparison of the full genome sequences obtained directly from the patient samples with the genome data obtained from the two SARS-CoV-2 isolates showed that the 21-nucleotide deletion was present in a minority of sequencing reads (1%) in the genome obtained from the patient sample from day 49 (Table 2), and was selected for upon passage in cell culture. The 12-nucleotide deletion at day 70 was present in 100% of the reads in both the clinical sample and tissue culture

isolate. Notably, neither spike deletion was detected in the genome sequences from the day 85 and day 105 swabs (Table 2). It is possible that other minor variants exist at low levels that were undetected by the depth of sequencing coverage or were not reflected in the sampling at that timepoint. The variation observed between the different full-length genomes obtained at various time-points during the course of infection points to a quasispecies complex with continuous turnover of dominant viral species.

Growth kinetics of SARS-CoV-2 patient isolates

The replication kinetics of the day 49 isolate SARS-CoV-2 were compared to those of the reference strain USA/WA1/2020 in Vero E6 cells. Despite the observed mutations in the day 49 isolate, no difference in replication kinetics were observed between the day 49 isolate and the reference strain (Figure 6A). To determine growth kinetics in a more functionally relevant cell type, growth curves were also performed on primary human alveolar epithelial tissues (EpiAlveolar^{TM}, MatTek Corporation, Ashland, MA, USA). No significant differences were observed between the patient isolate and reference strain in these cells either (Figure 6B).

Discussion

In this report, we describe long-term SARS-CoV-2 shedding in an immunocompromised patient with chronic lymphocytic leukemia (CLL) and acquired hypogammaglobulinemia out to 105 days past the initial positive test. Although the exact time-point when the patient acquired the SARS-CoV-2 is unknown, it is likely that the exposure occurred in the long-term care facility where she resided between February 19-25, 2020, just shortly before a large COVID-19 outbreak was identified in that facility on February 28, 2020. The patient remained asymptomatic throughout the

course of infection despite the isolation of infectious SARS-CoV-2 49 and 70 days past the initial diagnosis, much longer than shedding of infectious virus up to day 20 as reported previously (van Kampen et al., 2020). The information available to date on SARS-CoV-2 infection in immunocompromised patients, including those with cancers such as CLL, is limited, and mostly focuses on disease severity and outcome (He et al., 2020a, Paneesha et al., 2020, Baumann et al., 2020, Furstenau et al., 2020, Jin et al., 2020, Soresina et al., 2020, Zhu et al., 2020, Fill et al., 2020). Although it is difficult to extrapolate from a single patient, our data suggest that long-term shedding of infectious virus may be a concern in certain immunocompromised patients. Given that immunocompromised patients could have prolonged shedding and may not have typical symptoms of COVID-19, symptom-based strategies for testing patients and discontinuing transmission-based precautions, as recommended by the CDC (CDC, 2020b), may fail to detect whether certain patients are shedding infectious virus.

The patient eventually cleared the SARS-CoV-2 infection from the upper respiratory tract, after the development of low neutralizing antibody titers. How the virus was cleared and the effect of convalescent plasma on clearance of virus is unknown. The initial administration of convalescent plasma was followed by a decreased viral load in nasal swabs, but viral loads subsequently increased, despite administration of a second dose of convalescent plasma comprising higher antibody titers. Therapeutic administration of convalescent plasma is focused at treatment of severe or life-threatening COVID-19. Several clinical trials are investigating the efficacy of convalescent plasma, but currently the efficacy of convalescent plasma therapy on COVID-19 outcome remains equivocal (Mira et al., 2020, Salazar et al., 2020). The limited impact of the convalescent plasma treatment on clearance of SARS-CoV-2 could be due to the fact that IV

administered antibodies do not distribute well to the nasal epithelium (Ikegami et al., 2020) compared to the lower respiratory tract (Mira et al., 2020).

Throughout the course of infection there was marked within-host genomic evolution of SARS-CoV-2. Deep sequencing revealed a continuously changing virus population structure with turnover in relative frequency of the observed genotypes over the course of infection. Within SARS-CoV-2 there is generally relatively limited within-host variation reported, and over the course of infection the major SARS-CoV-2 population remains identical (Jary et al., 2020, Shen et al., 2020, Capobianchi et al., 2020). Potential factors contributing to the observed within-host evolution is the prolonged infection and the compromised immune status of the host, possibly resulting in a different set of selective pressures compared to an immune-competent host. These differential selective pressures may have allowed a larger genetic diversity with a continuous turnover of dominant viral species throughout the course of the infection. While some sequence variants remain consistent throughout the duration of infection, we also observed variants unique to individual time points, such as the spike deletions observed at day 49 and day 70. Previously reported spike deletions, distinct from those reported herein, were observed at relatively low frequency in clinical samples, but were enriched upon virus isolation (Andres et al., 2020, Liu et al., 2020d). Similar to these reports, the spike deletion in the isolate at day 49 was observed as a minor variant in the patient sample but was also selected for during passage upon virus isolation.

In contrast to the previously reported deletions at the cleavage sites, both spike deletions observed at day 49 and 70 in the patient are located in the NTD of S1, a region distal from the receptor binding site. These deleted residues are not modelled in a number of spike structures (Wrapp et al.,

2020, Walls et al., 2020), suggesting that this region is conformationally labile. Although the NTD has been identified as an antigenic target (Brouwer et al., 2020, Chi et al., 2020, Liu et al., 2020a), no clear difference in virus neutralization was observed between the two patient isolates and the prototype USA/WA1/2020 SARS-CoV-2 isolate.

Despite genetic changes in the SARS-CoV-2 isolated from the patient, replication kinetics did not significantly change when compared to the USA/WA1/2020 virus in Vero E6 cells and primary human alveolar epithelial tissues. This indicates that, most likely, the infectious virus shed by the patient would still be able to establish a productive infection in contacts upon transmission, assuming that viral growth kinetics *in vitro* are a suitable surrogate for virus fitness *in vivo*. Moreover, despite prolonged replication exclusively in the upper respiratory tract, the virus was still able to replicate in epithelial cells derived from the lower respiratory tract, suggestive that it could still cause pneumonia.

Many current infection control guidelines assume that persistently PCR positive patients are shedding residual RNA and not infectious virus, with immunocompromised patients thought to remain infectious for no longer than 20 days after symptom onset (CDC, 2020a). Here, we show that certain patients may shed infectious, replication-competent virus for much longer durations than previously recognized (van Kampen et al., 2020). Whereas infectious virus could be detected up to day 70, sgRNA, a molecular marker for active SARS-CoV-2 replication (Speranza et al., 2020), could be detected up until day 105. An immunocompromised state has been identified as a risk factor for the development of severe disease and complications from COVID-19 (CDC, 2020b). A wide variety of conditions and treatments can alter the immune system and cause

immunodeficiency, creating opportunities for prolonged viral replication and shedding of infectious SARS-CoV-2. While this reports focuses on the long-term shedding of one immunocompromised patient, an estimated 3 million people in the US have some form of immunocompromising condition, including HIV infection, solid-organ transplant recipients, haemopoietic stem-cell transplants, patients receiving chemotherapy and patients receiving corticosteroids (Kunisaki and Janoff, 2009). This transient or chronic immunocompromised patient population is at higher risk of respiratory disease complications with respiratory infections such as influenza A virus and SARS-CoV-2 (Kunisaki and Janoff, 2009). Prolonged shedding of pH1N1 shedding was observed in immunocompromised patients with a variety of immunocompromising conditions during the previous pandemic in 2009, such as cancer patients on chemotherapy and solid-organ transplant recipients (van der Vries et al., 2013). For the SARS-CoV-2 related Middle East respiratory syndrome coronavirus (MERS-CoV), prolonged shedding up to 38 days was observed in patients with myelodysplastic syndrome, autologous peripheral blood stem cell transplantation for treatment of large B-cell lymphoma and a patient with a peripheral T-cell lymphoma (Kim et al., 2017). MERS-CoV shedding was higher and longer in experimentally infected non-human primates immunosuppressed with cyclophosphamide and dexamethasone providing experimental support for the impact of immunosuppression on virus-host dynamics observed here (Prescott et al., 2018).

Limitations of the Study

A limitation of the present study is that it comprises only a single case, making it difficult to draw general conclusions on the use of convalescent plasma in clearance of the virus, potential alternative mechanisms involved in virus clearance and the frequency of persistent SARS-CoV-2

infection and shedding in patients with other immunocompromising conditions. Identification of additional cases of persistent infection and long-term shedding of infectious virus are needed so the infection dynamics can be studied in this diverse population in more detail. Understanding the mechanism of virus persistence and eventual clearance will be essential to providing appropriate treatment and preventing transmission of SARS-CoV-2, as persistent infection and prolonged shedding of infectious SARS-CoV-2 might occur more frequently. Because immunocompromised patients are often cohorted in hospital settings, a more nuanced approach to testing these individuals is warranted, and the presence of persistently positive patients by performing SARS-CoV-2 gRNA and sgRNA analyses on clinical samples should be investigated.

Acknowledgements

We would like to thank Neeltje van Doremalen, Jonathan Schulz, Myndi Holbrook, Anita Mora and Rose Perry for excellent technical assistance. We would like to thank MatTek corporation for providing the alveolar tissue culture system and technical support, as well as all the originating and submitting laboratories and authors who deposited SARS-CoV-2 genomes to GISAID. We would also like to thank the health care workers and laboratorians at EvergreenHealth for the selfless service to patients. Finally, to the patient described in this report for her gracious willingness to participate and contribute to these studies as we sought to understand this enigmatic infection.

Funding

This work was supported by the Intramural Research Program of the National Institute of Allergy and Infectious Diseases (NIAID). T.A.B. is supported by the Medical Research Council UK

(MR/S007555/1). The Wellcome Centre for Human Genetics is supported by Wellcome Centre grant 203141/Z/16Z.

Author Contributions

Conceptualization, F.X.R and V.J.M.; Resources, E.R.F., C.M., and F.X.R.; Methodology, V.A.A., M.J.M., S.N.S., B.N.W, E.R.F, C.M., T.A.B. and E.D.W.; Investigation, V.A.A, M.J.M, S.N.S, R.P., B.N.W., S.A., K.B., E.R.F., and E.D.W.; Writing – Original Draft, V.A.A., M.J.M, F.X.R. and V.J.M; Writing –Review & Editing, S.N.S., S.D.J., C.M., T.A.B., E.D.W.; Data Curation, C.M.; Supervision, T.A.B., E.D.W., F.X.R., and V.J.M..

Declaration of Interests

The authors declare no competing interests.

Figure Titles and Legends

Figure 1. Timeline of clinical presentation, diagnostic tests, and treatments of an immunocompromised patient with long term shedding of SARS-CoV-2. Dates of relevant clinical events, such as surgeries, therapies, and outcome of diagnostic tests are shown. Diagnostic qRT-PCR positive nasopharyngeal and oropharyngeal swabs taken 49, 70, 77, 85, and 105 days from the initial positive patient sample were sent to Rocky Mountain Laboratories, NIH, for further analysis. Serum and plasma samples pre and post transfusion, as well as a sample from the donor plasma, were also provided. See also Tables S1-S3 for additional laboratory values and clinical information.

Figure 2. Assessment of viral load and seroconversion in a patient persistently infected with SARS-CoV-2 and treated with convalescent plasma. (A) Viral loads were in nasopharyngeal swabs collected at different timepoints after the initial SARS-CoV-2 diagnosis. Viral RNA extracted from nasopharyngeal swab was analyzed for the presence of genomic RNA (gRNA; dark blue) and subgenomic RNA (sgRNA; light blue symbols) by qRT-PCR and reported as Ct value (circles, left panel) and in droplet digital PCR and reported as copy numbers (triangles, right panel). (B) IgG titers against full length recombinant SARS-CoV-2 spike ectodomain were determined in ELISA on convalescent plasma used for transfusion. The light grey bar is the IgG titer of the fist donor (convalescent plasma 1) and the dark grey is the second donor (convalescent plasma 2). (C) IgG titers against full length recombinant SARS-CoV-2 spike ectodomain were determined in ELISA on patient serum collected on several timepoints, including immediately before and after transfusion with convalescent plasma at day 71 (light grey) and 82 (dark grey). Each serum/plasma sample was tested in duplicate. See also Figure S1 for IgG titers against SARS-CoV-2 receptor binding domain (RBD).

Figure 3. Electron microscopy confirms isolation of coronavirus from patient nasopharyngeal swabs. SARS-CoV-2 cultured from patient nasopharyngeal swabs was used to inoculate Vero E6 cells for imaging by scanning and transmission electron microscopy (SEM and TEM). SEM images of the day 49 (A) and day 70 isolate (B). TEM images of the day 49 (C) and day 70 (D and E) isolate. SEM scalebar: 1 µM; TEM scalebar: 0.5 µM.

Figure 4. Phylogenomic analyses of described SARS-CoV-2 strains in a persistently infected patient. (A) Full genome SARS-CoV-2 sequences representing previously described lineages (Rambaut et al., 2020) were downloaded from GISAID (Shu and McCauley, 2017). Lineages were then assigned using Pangolin v2.0.3 (https://pangolin.cog-uk.io/). Using a representative genome from the assigned lineages and the four patient SARS-CoV-2 sequences, a maximum likelihood tree was inferred using PhyML v3.3.20180621 (Guindon et al., 2010) implemented in Geneious Prime v. 2020.1.2 (www.geneious.com) with a general time reversible model of nucleotide substitution and rooted at the Wuhan-Hu-1/2019 SARS-CoV-2 strain. Sequences from A and A.1 lineages are labelled, and the patient SARS-CoV-2 sequences are shown in cyan. hCoV-19/USA/WA-RML-1, 2, 3, and 4 are the patient derived genome sequences from day 49, 70, 85, and 105 nasopharyngeal swabs, respectively. (B) Full SARS-CoV-2 genomes were subsampled from Washington state representing NextStrain clade 19B, including the four full genome sequences recovered from the patient and the Wuhan-Hu-1/2019 sequence, and aligned using MAFFT v1.4 (Katoh and Standley, 2013, Katoh et al., 2002) implemented in Geneious Prime v. 2020.1.2 (www.geneious.com). A maximum likelihood tree was then reconstructed with PhyML v. 3.1 (Guindon et al., 2010) and a tree showing temporal divergence was inferred in TreeTime v. 0.7.6 (Hadfield et al., 2018). The patient SARS-CoV-2 sequences are shown in cyan and hCoV-19/USA/WA-RML-1, 2, 3, and 4 are the patient derived genome sequences from day 49, 70, 85, and 105 nasopharyngeal swabs, respectively. See also Figure S2.

Figure 5. Deletions in the N-terminal domain of S1 of the spike protein. (A) Nucleotide and amino acid sequence alignment of the region of the spike gene of the four patient sequences and

the reference USA/WA1/2020 genome sequence containing the deletions observed in the day 49 and day 70 samples. Alignment was generated with MAFFT v.1.4 (Katoh and Standley, 2013, Katoh et al., 2002) implemented in Geneious Prime 2020.1.2 (https://www.geneious.com). (B) Amino acid residues removed by the day 49 (orange) and day 70 (red) spike deletions are highlighted on a SARS-CoV-2 spike trimer (PDB: 6zge) (Wrobel et al., 2020). Each protomer of the trimer is shown in surface representation, colored in shades of grey. A single protomer is annotated and its secondary structure is shown in cartoon representation. Glycans are shown as beige-colored sticks. Previously reported spike deletions observed at the S1/S2 and S2' cleavage sites (Andres et al., 2020, Lau et al., 2020, Liu et al., 2020d) are colored blue and cyan, respectively. (C). Close-up view of the indicated region of panel B (dotted box) with the protein surface removed for clarity and accompanying amino acid sequence alignment, generated using Multalin (Corpet, 1988) and plotted with ESPript (Robert and Gouet, 2014).

Figure 6. Growth kinetics of the day 49 patient isolate in Vero E6 cells and primary human alveolar epithelial tissues. (A) Vero E6 cells were inoculated with the day 49 patient isolate and the reference USA/WA1/2020 strain at a MOI of 0.01, in triplicate. (B) Primary 3D human alveolar epithelial tissues grown in 3D transwell culture were inoculated with the same isolates at a MOI of 0.1. Supernatant was harvested at designated timepoints for assessment of viable virus using endpoint titration. Data shown are the mean and the standard error of the mean for three independent replicates. Statistical analysis using a 2-way ANOVA in GraphPad Prism shows no significant difference between the isolates at any of the timepoints.

Tables

Table 1. Virus neutralization titers in patient pre- and post-transfusion sera and convalescent plasma used for transfusion. Virus neutralization assays were performed for all sera and plasma with SARS-CoV-2 strains USA/WA1/2020 and the day 49 and day 70 patient isolates. Each serum/plasma sample was tested in duplicate.

Sera	USA/WA1/2020	Day 49 isolate	Day 70 isolate
Day 49	<10	<10	<10
Day 71	<10	<10	<10
Day 71 post transfusion	<10	<10	<10
Day 77	<10	<10	<10
Day 82	<10	10	<10
Day 82 post transfusion	10	10	15
Day 105	10	<10	<10
Convalescent plasma 1	60	40	40
Convalescent plasma 2	160	160	60

Table 2. Consensus sequence variants in patient clinical samples and SARS-CoV-2 isolates compared to reference USA/WA1/2020 (MN985325.1). *Note – Minor variants present in less than 50% of the reads were not included in the consensus, but these minor variants were included in the table to demonstrate their presence in clinical samples as well as the isolate.

Position	gene	Nucleotide change	Protein change	Day 49 Patient	Day 49 Isolate	Day 70 Patient	Day 70 Isolate	Day 85 Patient	Day 105 Patient
518 – 520	orf1ab	3 bp deletion	M → del	22%*	100%	100%	100%	-	-
2,113	orf1ab	C → T	None	-	-	100%	100%	-	-
4,084	orf1ab	C → T	None	87.5%	100%	-	-	-	97%
17,747	orf1ab	C → T	P → L	100%	100%	100%	100%	100%	100%
17,858	orf1ab	A → G	Y → C	100%	100%	100%	100%	100%	100%
19,420	orf1ab	T → C	S → P	72%	98%	-	-	-	92%
21,975 – 21,995	Spike	21 bp deletion	DPFLGVYY → D	1%*	100%	-	-	-	-
21,982 – 21,993	Spike	12 bp deletion	FLGVY → F	-	-	100%	100%	-	-
23,010	Spike	T → C	V → A	100%	100%	100%	100%	100%	99%
23,616	Spike	G → A	R → Q	-	-	-	95%	-	-
23,617	Spike	T → A		-	-	-	95%	-	-
26,526	M	G → T	A → S	-	-	16%*	100%	-	-
27,899	Orf8	A → T	K → N	-	-	100%	100%	-	-
29,308	N	T → A	N → K	-	-	-	-	56%	-
29,854	-	C → T	-	-	-	-	100%	-	-

Supplemental Figure Titles and Legends

Figure S1. ELISA titers against SARS-CoV-2 receptor binding domain (RBD). Related to Figure 2. (A) IgG titers against SARS-CoV-2 receptor binding domain (RBD) were determined in ELISA on convalescent plasma used for transfusion. The light grey bar is the IgG titer of the fist donor (convalescent plasma 1) and the dark grey is the second donor (convalescent plasma 2). (B) IgG titers against SARS-CoV-2 (RBD) were determined in ELISA on patient serum collected on several timepoints, including immediately before and after transfusion with convalescent plasma at day 71 (light grey) and day 82 (dark grey). Each serum/plasma sample was tested in duplicate.

Figure S2. Maximum-likelihood trees of the SARS-CoV-2 patient with other SARS-CoV-2 genomes circulating in Washington state at the times of sampling (April 20, May 11, May 26, and June 15, 2020). Related to Figure 4, Table 2. (A) Maximum likelihood tree using 1789 full genome SARS-CoV-2 sequences deposited to GISAID until 20 April 2020. Inset shows a close up of the monophyletic clade of the genomes directly obtained from the patient samples (cyan). (B) Maximum likelihood tree using 385 full genome SARS-CoV-2 sequences deposited to GISAID between 20 April and 11 May, 2020. The monophyletic clade of the genomes directly obtained from the patient samples is shown in cyan. (C) Maximum likelihood tree using 268 full genome SARS-CoV-2 sequences deposited to GISAID between 11 May and 26 May, 2020. The monophyletic clade of the genomes directly obtained from the patient samples is shown in cyan. (D) Maximum likelihood tree using 709 full genome SARS-CoV-2 sequences deposited to GISAID between 26 May and 15 June, 2020. The monophyletic clade of the genomes directly obtained from the patient samples is shown in cyan.

STAR Methods

Resource Availability

Lead Contact

Further information and requests for resources and reagents should be directed to and will be fulfilled by the Lead Contact, Vincent Munster (Vincent.munster@nih.gov).

Materials Availability

This study did not generate new reagents.

Data Availability

The data and the Supplementary Tables from this study have been deposited to Mendeley Data at http://dx.doi.org/10.17632/3n377gv8kb.

Genome sequences have been deposited to Genbank: MT982403, MT982402, MT982405, MT982406, MT982401 and MT982404.

Experimental Model and Subject Details

Human Patient

The patient described in this case study is a 71 year old female with a 10 year history of chronic lymphocytic leukemia (CLL), acquired hypogammaglobulinemia, anemia, and chronic leukocytosis. The patient tested positive for SARS-CoV-2 on March 2, 2020, and remained positive through June 15, 2020. During the course of the study, the patient was transfused with intravenous immunoglobulin (IVIG, 25 g) on April 6 and May 6, 2020, and convalescent plasma against SARS-CoV-2 on May 12 and May 23, 2020. After the initial SARS-CoV-2 diagnosis, the

patient was kept in isolation in an isolation ward in a single room with negative airflow. Anonymized plasma, serum and swabs from a patient at EvergreenHealth, Kirkland, Washington were obtained under an NIH Institutional Review Board exemption. Verbal and signed consent were obtained from the patient to allow analyses of the samples.

Cells

Vero E6 is a female African green monkey kidney epithelial cell line. Vero E6 cells were maintained at 37°C and 5% CO_2 in DMEM supplemented with 10% fetal bovine serum, 1 mM L-glutamine, 50 U/mL penicillin and 50 µg/mL streptomycin. Vero E6 cells were provided by Dr. Ralph Baric. Cells were authenticated by cytochrome B sequencing. Mycoplasma testing was performed monthly, and no mycoplasma was detected.

FreeStyle 293-F (RRID: CVCL_D603) is a female human embryonic cell line adapted for growth in suspension culture. FreeStyle 293-F cells were grown in Freestyle 293 Expression Medium (Gibco) at 37°C and 8% CO_2, shaking at 130 rpm. Cells were not authenticated in house. Mycoplasma testing was performed monthly, and no mycoplasma was detected.

MatTek EpiAlveolar is a 3D co-culture model of the air-blood barrier produced from primary human alveolar epithelial cells, pulmonary endothelial cells and fibroblasts, and maintained according to manufactures instructions (https://www.mattek.com/products/epialveolar/). Cells were not authenticated in house. Mycoplasma testing was performed monthly, and no mycoplasma was detected.

538

539 *SARS-CoV-2 Virus*

540 SARS-CoV-2 strain nCoV-WA1-2020 (MN985325.1) (Harcourt et al., 2020) was provided by
541 CDC, Atlanta, USA. SARS-CoV-2 isolates were propagated on Vero E6 cells grown in DMEM
542 supplemented with 2% fetal bovine serum (Gibco), 1 mM L-glutamine (Gibco), 50 U/mL
543 penicillin and 50 µg/mL streptomycin (Gibco) (virus isolation medium), at 37°C and 5% CO_2.

544

545 Infectious titer of SARS-CoV-2 virus stocks was determined by end-point titration and is
546 reported as $\log_{10}$ 50% tissue culture infective dose ($TCID_{50}$/mL). 1.5 x 10^4 Vero E6 cells were
547 seeded into each well in 96-well plates in DMEM supplemented with 10% fetal bovine serum, 1
548 mM L-glutamine, 50 U/mL penicillin and 50 µg/mL streptomycin and incubated overnight at
549 37°C and 5% CO_2. The following morning, when the cells were at approximately 90%
550 confluency, the wells were inoculated with ten-fold serial dilutions of virus stock diluted in virus
551 isolation medium (100 uL per well, with 10 replicate wells for each dilution). The plates were
552 incubated at 37°C and 5% CO_2, and the cytopathic effect (CPE) was assessed for each well after
553 5 days. Wells that demonstrated CPE were counted, and the titer was determined by the method
554 of Spearman and Kärber using 10 replicates as follows:

555 $$\text{Log}_{10}\ TCID_{50}/mL = (X - d/2 + [d \bullet S])$$

556 where X is $\log_{10}$ of the lowest dilution with all wells positive for CPE, d is $\log_{10}$ of the dilution
557 factor (10 in these titrations), and S is the sum of the fraction of wells positive for CPE at all
558 tested dilutions.

559

560 **Method Details**

Clinical Sample RNA Extraction and qRT-PCR

Clinical samples were deidentified as part of their analyses. Nasopharyngeal and oropharyngeal swabs were shipped on wet ice in viral transport medium (VTM) to Rocky Mountain Laboratories (NIH). RNA was extracted using Trizol (Invitrogen), Phasemaker tubes (Invitrogen) and the PureLink RNA Mini Kit (Invitrogen) according to manufacturer's instructions and eluted in 100 µL RNase-free H2O. First strand cDNA synthesis was performed with the SuperScript IV First Strand Synthesis System (Invitrogen), using 11 µL input RNA and random hexamers. qRT-PCR was performed using 5 µL of cDNA using the QuantiFast Probe kit (QIAGEN) using E gRNA (Corman et al., 2020) and sgRNA specific assays (Wolfel et al., 2020). To quantify viral load within the patient samples, 5 µL of cDNA was analyzed using droplet digital PCR (Biorad) using the same E gRNA and sgRNA assays. The SARS-CoV-2 testing through EvergreenHealth were performed by University of Washington, LabCrop, Cepheid, and GenMark. Kashi clinical laboratories and Magnolia diagnostics performed the negative tests taken at the care facilities.

Virus Isolation

Virus isolation of the clinical specimen was performed on Vero E6 cells in 96 well plates. In brief, media was removed from wells and replaced with 100 µL of undiluted swab sample, or swab sample diluted 1:10 in DMEM supplemented with 2% fetal bovine serum (Gibco), 1 mM L-glutamine (Gibco), 50 U/mL penicillin and 50 µg/mL streptomycin (Gibco) (virus isolation medium). Diluted and undiluted samples were inoculated onto 7 wells. Spin inoculation was performed at 1000 x g for 1 hour at 35°C. Inoculum was removed and wells were washed twice with and replaced with 100 µL of virus isolation medium and incubated at 37°C and 5% CO_2.

584 After 5 days, replicate wells were pooled, diluted 10x in virus isolation medium, and used to
585 inoculate T25 flasks of Vero E6 cells in virus isolation medium and incubated at 37°C and 5%
586 CO_2. Flasks were observed for cytopathic effect. RNA was extracted, as described above, for
587 confirmation of SARS-CoV-2 by qRT-PCR and next generation sequencing.
588
589 *Growth kinetics of SARS-COV-2 isolates*
590 Vero E6 cells were seeded in 6 well plates at a density of 4 x 10^5 cells/well in DMEM
591 supplemented with 2% fetal bovine serum (Gibco), 1 mM L-glutamine (Gibco), 50 U/mL
592 penicillin and 50 µg/mL streptomycin (Gibco) (virus isolation medium) and incubated overnight
593 at 37°C and 5% CO_2. The following day, the media was removed from the wells and replaced
594 with 1 mL of virus isolation medium containing virus at a MOI of 0.01. The patient day49 isolate
595 and the USA/WA1/2020 strain were tested in triplicate, with mock control wells in triplicate.
596 After a 1-hour incubation at 37°C and 5% CO_2, the inoculum was removed, and wells were
597 washed 3x with PBS and replaced with a fresh 2 mL of virus isolation medium. Supernatant
598 samples were taken at 0, 12, 24, 48, 72, 96, and 120 hours post inoculation. Titer of infectious
599 virus from supernatant was determined by endpoint titration in Vero E6 cells, as described
600 above, but using 4 replicates per sample to determine the $TCID_{50}$/mL using the Spearman-Karber
601 method. The EpiAlveolar cell growth kinetic experiment was set up similar to the Vero E6 cells
602 but with the following differences. Cells were provided by MatTek with 2.5 x 10^5 cells/transwell
603 insert. Cells were infected by adding 75 µL of ALI medium containing virus at an MOI of 0.01
604 to the apical side of the transwell insert. After the above outlined incubation, the inoculum was
605 removed, wells were washed 1x with PBS and replaced with 75 µL of ALI medium upon the
606 apical surface. During sampling of the EpiAlveolar cells, 500 µL of DMEM medium was added

607 to the apical side, gently pipetted to mix, removed, and 75 µL of fresh ALI medium replaced on
608 the apical surface.
609
610 *Expression and Purification of SARS-CoV-2 Spike and Receptor Binding Domain*
611 Expression plasmids encoding the codon optimized SARS-CoV-2 full length spike and receptor
612 binding domain (RBD) were kindly provided Kizzmekia Corbett and Barney Graham (Vaccine
613 Research Center, Bethesda, USA) and Florian Krammer (Icahn School of Medicine at Mt. Sinai,
614 New York, USA), respectively (Wrapp et al., 2020, Amanat et al., 2020). Both plasmids were
615 expressed in Freestyle 293-F cells (Thermofisher), maintained in Freestyle 293 Expression
616 Medium (Gibco/ThermoFisher) at 37°C and 8% CO_2 in a humidified incubator shaking at 130
617 rpm. Cultures totaling 500 mL were transfected with PEI at a density of one million cells per
618 mL. Supernatant was harvested 7 days post transfection, clarified by centrifugation and sterile
619 filtered through a 0.22 µM membrane. The protein was purified using Ni-NTA immobilized
620 metal-affinity chromatography (IMAC) using Ni Sepharose 6 Fast Flow Resin (GE Lifesciences)
621 or NiNTA Agarose (QIAGEN) and gravity flow. After elution the protein was buffer exchanged
622 into 10 mM Tris pH8, 150 mM NaCl buffer before further use or frozen at -80°C for storage.
623
624 *Enzyme-Linked Immunosorbent Assay (ELISA)*
625 Purified SARS-CoV-2 full length spike or RBD protein was diluted to 1 µg/mL in PBS.
626 Maxisorp plates (Nunc) were coated with 100 µL per well (100 ng protein per well) and
627 incubated overnight at 4°C. Plates were washed 3x with PBST (0.1% Tween) and blocked with
628 100 µL casein in PBS blocking buffer (ThermoFisher) for 1 hour at room temp. Plates were
629 again washed 3x with PBST (0.1% Tween), and 100 µL of serum samples, serially diluted 2 fold

630 in casein in PBS blocking buffer, in duplicate, was added to the wells and incubated at room
631 temperature for 1 hour. Plates were washed 4x with PBST (0.1% Tween), and 100 µL secondary
632 antibody, rabbit anti-human IgG Fc HRP (Novus Biologicals, NBP1-73529) diluted 1:4000 in
633 casein in PBS blocking buffer, was added to the wells and incubated for 1 hour at room
634 temperature. The wells were washed 5x with PBST (0.1% Tween) and developed with the KPL
635 TMP 2-component peroxidase substrate kit (Seracare, 5120-0047). The reaction was stopped
636 with KPL stop solution (Seracare, 5150-0020) and read at 450 nm. The threshold for positivity
637 was calculated as the average plus 3 times the standard deviation of negative control sera.
638 Reported titers are the reciprocal value of the highest dilution at which signal was observed
639 above the calculated threshold.
640
641 *Virus Neutralization assay*
642 Serum and plasma samples were heat inactivated at 56°C for 30 minutes. Two-fold serial
643 dilutions were prepared in DMEM supplemented with 2% FBS, with each sample diluted in
644 duplicate in 96 well plate format. 100 $TCID_{50}$ of SARS-CoV-2, in virus isolation medium, was
645 then added to each well. The virus-serum/plasma mixture was incubated at 37°C for 1 hour to
646 allow for neutralization, then 100 uL per well was added to Vero E6 cells in 96 well plates and
647 incubated at 37°C and 5% CO_2. After 5 days, wells were observed for cytopathic effect. The
648 virus neutralization titer is displayed as the reciprocal value of the highest dilution of
649 serum/plasma that still inhibited virus replication at which no cytopathic effect was observed.
650
651 *Next generation sequencing of patient clinical samples and isolates*

Clinical Samples - Viral RNA was extracted from patient nasopharyngeal swabs using Trizol (Invitrogen) for use with the ARTIC nCoV-2019 sequencing protocol V.1 (Protocols.io - https://www.protocols.io/view/ncov-2019-sequencing-protocol-bbmuik6w). 30-35 PCR cycles were used to generate tiled-PCR amplicons. Primer pools consisted of the ARTIC nCoV-2019 v3 Panel (Integrated DNA Technologies, Belgium) and were diluted and used in PCR reactions following the instructions. Products from Pool 1 and Pool 2 were combined, AmPure XP cleaned, and quantitated as per the instructions – through step 16.18. Following assessment on a BioAnalyzer DNA Chip (Agilent Technologies, Santa Clara, CA), a volume consisting of 500 ng of product was taken directly into TruSeq DNA PCR-Free Library Preparation Guide, Revision D. (Illumina, San Diego, CA) beginning with the Repair Ends step (q.s. to 50 µL with RSB) and subsequent cleanup consisted of a single 1:1 AmPure XP/reaction ratio. All downstream steps followed the manufacturer's instructions. Final libraries were visualized on a BioAnalyzer HS chip (Agilent Technologies, Santa Clara, CA) and quantified using KAPA Library Quant Kit (Illumina) Universal qPCR Mix (Kapa Biosystems, Wilmington, MA) on a CFX96 Real-Time System (BioRad, Hercules, CA).

Isolates - Viral RNA was extracted from clarified cell culture supernatant using Trizol (Invitrogen). Extracted RNA was depleted of rRNA using Ribo-Zero Gold H/M/R (Illumina, San Diego, CA) based on manufacturer’s protocols. After Ampure RNAClean XP (Beckman Coulter, Brea, CA) purification, the enriched RNA was eluted in 6 µL of water and assessed on a BioAnalyzer RNA Pico Chip (Agilent Technologies, Santa Clara, CA). Following the Truseq Stranded mRNA Library Preparation Guide, Revision E., (Illumina, San Diego, CA), the remaining RNA was added to Elute-Frag-Prime Buffer and continued through second-strand

cDNA synthesis. The resulting double-stranded cDNAs were treated with a combined mixture of RiboShredder RNase Blend (Lucigen, Middleton, WI) and high concentration DNase-free RNase (Roche Diagnostics, Indianapolis, IN). After AMpure XP purification (Beckman Coulter, Brea, CA), samples were analyzed on a RNA Pico chip to confirm no remaining RNA. Library preparation continued with adenylation of ends following manufacturer's recommendations. All downstream steps followed the manufacturer's instructions. Final libraries were visualized on a BioAnalyzer DNA1000 chip (Agilent Technologies, Santa Clara, CA) and quantified using KAPA Library Quant Kit (Illumina) Universal qPCR Mix (Kapa Biosystems, Wilmington, MA) on a CFX96 Real-Time System (BioRad, Hercules, CA).

Sequencing and bioinformatics

Libraries were diluted to 2 nM stock, pooled together as needed in equimolar concentrations and sequenced on the MiSeq (Illumina, Inc, San Diego, CA) using on-board cluster generation and 2 x 150 paired-end sequencing. Raw image files were converted to fastq files using bcl2fastq (v2.20.0.422, Illumina, Inc. San Diego, CA) and trimmed of adapter sequences using cutadapt version 1.12 (Martin, 2011). Adapter-trimmed reads were trimmed and filtered to remove low quality sequence using fastq_quality_trimmer and fastq_quality_filter tools from the FASTX Toolkit, v 0.0.14 (Gordon, Gordon, 2018). Singletons were removed and quality filtered reads were coordinate-order sorted using a custom perl script.

Reads were filtered for repeat sequence, rRNA, and PhiX contaminants and then mapped to the SARS-CoV-2 isolate 2019-nCoV/USA_WA1 (MN985325.1) reference genome using bowtie2 with –no-mixed –no-unal -X 1500 options (Langmead and Salzberg, 2012). Aligned SAM files were converted to BAM format, then sorted and indexed using SAMtools (Li et al., 2009).

Duplicate reads were removed from the mapped reads using picard's MarkDuplicates tool (Institute, 2018)

To process the ARTIC data a custom pipeline was developed. Fastq read pairs were first compared to a database of ARTIC primer pairs to identify read pairs that had correct, matching primers on each end. Once identified, the ARTIC primer sequence was trimmed off. Read pairs that did not have the correct ARTIC primer pairs were discarded. Remaining read pairs were collapsed into one sequence using AdapterRemoval (Schubert et al., 2016), requiring a minimum 25 base overlap and 300 base minimum length, generating ARTIC amplicon sequences. Identical amplicon sequences were removed and the unique amplicon sequences were then mapped to the SARS-CoV-2 genome (MN985325.1) using Bowtie2 (Langmead and Salzberg, 2012). Aligned SAM files were converted to BAM format, then sorted and indexed using SAMtools (Li et al., 2009).

Variant calling was performed using Genome Analysis Toolkit (GATK, version 4.1.2) HaplotypeCaller with ploidy set to 2 (McKenna et al., 2010). Single nucleotide polymorphic variants were filtered for QUAL > 200 and quality by depth (QD) > 20 and indels were filtered for QUAL > 500 and QD > 20 using the filter tool in bcftools, v1.9 (Li et al., 2009). The accuracy of the filtered variant calls was manually inspected in Broad's Integrative Genomics Viewer (IGV) (Robinson et al., 2017). Consensus sequences were generated using bcftools consensus (Li et al., 2009) and subsequently aligned using MAFFT (Katoh and Standley, 2013, Katoh et al., 2002) with 2,434 GISAID Washington SARS2 reference sequences in addition to the 2019-nCoV/USA_WA1 genome used for mapping.

Phylogenomic Analysis

Available SARS-CoV-2 full genome sequences were downloaded from the GISAID database (http://gisaid.org/) (Shu and McCauley, 2017). The sequences were then assigned to previously described lineages (Rambaut et al., 2020) using Pangolin v2.0.3 (https://pangolin.cog-uk.io/), and aligned using MAFFT v. 1.4 (Katoh and Standley, 2013, Katoh et al., 2002). A maximum likelihood tree with the patient SARS-CoV-2 genomes, the Wuhan-Hu-1/2019 genome sequence, the USA/WA-1/2020 genome, and a representative genome from the assigned lineages was inferred using PhyML v.3.3.20180621 (Guindon et al., 2010) implemented in Geneious Prime v.2020.1.2 (www.geneious.com) with a general time reversible model of nucleotide substitution and rooted at the Wuhan-Hu-1/2019 SARS-CoV-2 strain. The final figure was made using FigTree v.1.4.4 (http://tree.bio.ed.ac.uk/software/figtree/). For the time tree, full SARS-CoV-2 genomes were subsampled from Washington state representing NextStrain clade 19B, including the four patient genomes sequences and the Wuhan-Hu-1/2019 genome sequence. The sequences were aligned using MAFFT v. 1.4 (Katoh and Standley, 2013, Katoh et al., 2002) implemented in Geneious Prime v. 2020.1.2 (www.geneious.com), a maximum likelihood tree reconstructed with PhyML v.3.1 (Guindon et al., 2010), and the time tree showing temporal divergence inferred in TreeTime v.0.7.6 (Hadfield et al., 2018) using the HKY85 model of nucleotide substitution and a fixed molecular clock at 8e-4 with a standard deviation of 4e-4 as implemented in the NextStrain pipeline (nextstrain.org/sars-cov-2/).

To evaluate the relationship between the SARS-CoV-2 genomes recovered from the patient swabs with other SARS-CoV-2 genomes from Washington state, genomes at the times of sampling (April 20, May 11, May 26, and June 15, 2020) from Washington state were downloaded from the GISAID database (http://gisaid.org) (Shu and McCauley, 2017). The sequences were aligned by MAFFT (Katoh and Standley, 2013, Katoh et al., 2002). The

744 sequences were analyzed by the Nextclade server v0.7.5 (https://clades.nextstrain.org/) for
745 quality and sequences that were not of sufficient quality were discarded. 1,789 sequences at
746 April 20, 385 sequences between April 20 and May 11, 268 sequences between May 11 and May
747 26, and 709 sequences between May 26 and June 15 were kept for further phylogenetic analysis.
748 Maximum likelihood trees using the curated sets of genomes, the four patient genomes, and the
749 USA/WA1/2020 genome, were inferred using ModelFinder (Kalyaanamoorthy et al., 2017) and
750 ultrafast bootstrap (Hoang et al., 2018) implemented in IQ-TREE (Nguyen et al., 2015), and
751 rooted at USA/WA1/2020. Final figures were made using FigTree v.1.4.4
752 (http://tree.bio.ed.ac.uk/software/figtree/). A table of acknowledgements for the GISAID genome
753 sequences used to within this work is available at Mendeley Data at
754 http://dx.doi.org/10.17632/3n377gv8kb.
755
756 *Electron Microscopy*
757 Vero E6 cells cultured in DMEM supplemented with 10% fetal bovine serum, 1 mM L-
758 glutamine, 50 U/mL penicillin and 50 µg/mL streptomycin were plated at 5 x 10^4 cells/well in 24
759 well plates containing Thermanox™ cover slips (Ted Pella, Redding, CA) for transmission
760 electron microscopy or silicon chips (Ted Pella, Redding, CA) for scanning electron microscopy
761 in the wells, and incubated overnight at 37°C and 5% CO_2. The next day, media was carefully
762 aspirated from the wells and replaced with 1 mL of virus isolation medium containing SARS-
763 CoV-2 virus at a MOI of 1 and incubated for 1 hour at 37°C and 5% CO_2. Wells were washed
764 three times with PBS, then replaced with 1 ml fresh virus isolation medium and incubated at
765 37°C and 5% CO_2. At 24 and 48 hours post-infection, wells were washed three times with PBS,
766 then fixed as described below.

Scanning electron microscopy

Cells were fixed with Karnovsky's formulation of 2% paraformaldehyde/2.5% glutaraldehyde in 0.1 M Sorenson's phosphate buffer, and then post-fixed with 1.0% osmium tetroxide/0.8% potassium ferrocyanide in 0.1 M sodium cacodylate buffer washed with 0.1 M sodium cacodylate buffer then stained with 1% tannic acid in dH2O. After additional buffer washes, the samples were further osmicated with 2% osmium tetroxide in 0.1M sodium cacodylate, then washed with dH2O. Specimens were dehydrated with a graded ethanol series from 50%, 75%, 100% x 3 for 5 minutes each, critical point dried under CO2 in a Bal-Tec model CPD 030 Drier (Balzers, Liechtenstein), mounted with double sided carbon tape on aluminum specimen mounts (Ted Pella), and sputter coated with 35 Å of iridium in a Quorum EMS300T D sputter coater (Electron Microscopy Sciences, Hatfield, PA) prior to viewing at 5 kV in a Hitachi SU-8000 field emission scanning electron microscope (Hitachi, Tokyo, Japan).

Transmission electron microscopy

Specimens were fixed as described above for scanning electron microscopy and additionally stained overnight with 1% uranyl acetate at 4 °C after the second osmium staining and then dehydrated with the same graded ethanol series and embedded in Spurr's resin. Thin sections were cut with a Leica UC7 ultramicrotome (Buffalo Grove, IL) prior to viewing at 120 kV on a FEI BT Tecnai transmission electron microscope (Thermofisher/FEI, Hillsboro, OR). Digital images were acquired with a Gatan Rio camera (Gatan, Pleasanton, CA).

Structure Mapping

The Pymol Molecular Graphics System (https://www.schrodinger.com/pymol) was used to map the location of the observed deletions onto a SARS-CoV-2 spike structure (PDB: 6ZGE) (Wrobel et al., 2020). Nucleotide sequence alignments were generated using MAAFT align (Katoh and Standley, 2013, Katoh et al., 2002) implemented in Geneious Prime v.2020.1.2 (https://www.geneious.com) and amino acid sequence alignments were generated with Multalin (Corpet, 1988) and plotted with ESPript (Robert and Gouet, 2014).

Quantification and Statistical Analysis

Data and statistical analysis was performed using GraphPad Prism 8.2.0. Replicates and statistical details can also be found in the methods and figure legends. For ELISA and virus neutralization assays, the serum/plasma samples were diluted and tested in duplicate. For the growth curves, both virus isolates (day 49 patient isolate and USA/WA1/2020) were tested in three replicate wells for both Vero E6 cells and the primary human alveolar epithelial cells. The growth curve data shown are the mean and standard error of the mean for the three independent replicates. The statistical analysis was performed using a 2-way ANOVA in Graphpad Prism 8.2.0. Further methods to determine whether the data met assumptions of the statistical approach were not relevant for these analyses.

References

AMANAT, F., STADLBAUER, D., STROHMEIER, S., NGUYEN, T. H. O., CHROMIKOVA, V., MCMAHON, M., JIANG, K., ARUNKUMAR, G. A., JURCZYSZAK, D., POLANCO, J., BERMUDEZ-GONZALEZ, M., KLEINER, G., AYDILLO, T., MIORIN, L., FIERER, D. S., LUGO, L. A., KOJIC, E. M., STOEVER, J., LIU, S. T. H., CUNNINGHAM-RUNDLES, C., FELGNER, P. L., MORAN, T., GARCIA-SASTRE, A., CAPLIVSKI, D., CHENG, A. C., KEDZIERSKA, K., VAPALAHTI, O., HEPOJOKI, J. M., SIMON, V. & KRAMMER, F. 2020. A serological assay to detect SARS-CoV-2 seroconversion in humans. *Nat Med,* 26**,** 1033-1036.

ANDRES, C., GARCIA-CEHIC, D., GREGORI, J., PIÑANA, M., RODRIGUEZ-FRIAS, F., GUERRERO-MURILLO, M., ESPERALBA, J., RANDO, A., GOTERRIS, L., CODINA, M. G., QUER, S., MARTÍN, M. C., CAMPINS,

M., FERRER, R., ALMIRANTE, B., ESTEBAN, J. I., PUMAROLA, T., ANTÓN, A. & QUER, J. 2020. Naturally occurring SARS-CoV-2 gene deletions close to the spike S1/S2 cleavage site in the viral quasispecies of COVID19 patients. *bioRxiv***,** 2020.06.03.129585.

BAUMANN, T., DELGADO, J. & MONTSERRAT, E. 2020. CLL and COVID-19 at the Hospital Clinic of Barcelona: an interim report. *Leukemia,* 34**,** 1954-1956.

BHATRAJU, P. K., GHASSEMIEH, B. J., NICHOLS, M., KIM, R., JEROME, K. R., NALLA, A. K., GRENINGER, A. L., PIPAVATH, S., WURFEL, M. M., EVANS, L., KRITEK, P. A., WEST, T. E., LUKS, A., GERBINO, A., DALE, C. R., GOLDMAN, J. D., O'MAHONY, S. & MIKACENIC, C. 2020. Covid-19 in Critically Ill Patients in the Seattle Region - Case Series. *N Engl J Med,* 382**,** 2012-2022.

BROUWER, P. J. M., CANIELS, T. G., VAN DER STRATEN, K., SNITSELAAR, J. L., ALDON, Y., BANGARU, S., TORRES, J. L., OKBA, N. M. A., CLAIREAUX, M., KERSTER, G., BENTLAGE, A. E. H., VAN HAAREN, M. M., GUERRA, D., BURGER, J. A., SCHERMER, E. E., VERHEUL, K. D., VAN DER VELDE, N., VAN DER KOOI, A., VAN SCHOOTEN, J., VAN BREEMEN, M. J., BIJL, T. P. L., SLIEPEN, K., AARTSE, A., DERKING, R., BONTJER, I., KOOTSTRA, N. A., WIERSINGA, W. J., VIDARSSON, G., HAAGMANS, B. L., WARD, A. B., DE BREE, G. J., SANDERS, R. W. & VAN GILS, M. J. 2020. Potent neutralizing antibodies from COVID-19 patients define multiple targets of vulnerability. *Science,* 369**,** 643-650.

BULLARD, J., DUST, K., FUNK, D., STRONG, J. E., ALEXANDER, D., GARNETT, L., BOODMAN, C., BELLO, A., HEDLEY, A., SCHIFFMAN, Z., DOAN, K., BASTIEN, N., LI, Y., VAN CAESEELE, P. G. & POLIQUIN, G. 2020. Predicting infectious SARS-CoV-2 from diagnostic samples. *Clin Infect Dis*.

BURBELO, P. D., RIEDO, F. X., MORISHIMA, C., RAWLINGS, S., SMITH, D., DAS, S., STRICH, J. R., CHERTOW, D. S., DAVEY, R. T., JR. & COHEN, J. I. 2020. Detection of Nucleocapsid Antibody to SARS-CoV-2 is More Sensitive than Antibody to Spike Protein in COVID-19 Patients. *medRxiv*.

CAPOBIANCHI, M. R., RUECA, M., MESSINA, F., GIOMBINI, E., CARLETTI, F., COLAVITA, F., CASTILLETTI, C., LALLE, E., BORDI, L., VAIRO, F., NICASTRI, E., IPPOLITO, G., GRUBER, C. E. M. & BARTOLINI, B. 2020. Molecular characterization of SARS-CoV-2 from the first case of COVID-19 in Italy. *Clin Microbiol Infect,* 26**,** 954-956.

CDC. 2020a. *Duration of Isolation and Precautions for Adults with COVID-19* [Online]. Available: https://www.cdc.gov/coronavirus/2019-ncov/hcp/duration-isolation.html [Accessed].

CDC. 2020b. *People with Certain Medical Conditions* [Online]. [Accessed August 31 2020].

CHI, X., YAN, R., ZHANG, J., ZHANG, G., ZHANG, Y., HAO, M., ZHANG, Z., FAN, P., DONG, Y., YANG, Y., CHEN, Z., GUO, Y., ZHANG, J., LI, Y., SONG, X., CHEN, Y., XIA, L., FU, L., HOU, L., XU, J., YU, C., LI, J., ZHOU, Q. & CHEN, W. 2020. A neutralizing human antibody binds to the N-terminal domain of the Spike protein of SARS-CoV-2. *Science,* 369**,** 650-655.

CORMAN, V. M., LANDT, O., KAISER, M., MOLENKAMP, R., MEIJER, A., CHU, D. K., BLEICKER, T., BRUNINK, S., SCHNEIDER, J., SCHMIDT, M. L., MULDERS, D. G., HAAGMANS, B. L., VAN DER VEER, B., VAN DEN BRINK, S., WIJSMAN, L., GODERSKI, G., ROMETTE, J. L., ELLIS, J., ZAMBON, M., PEIRIS, M., GOOSSENS, H., REUSKEN, C., KOOPMANS, M. P. & DROSTEN, C. 2020. Detection of 2019 novel coronavirus (2019-nCoV) by real-time RT-PCR. *Euro Surveill,* 25.

CORPET, F. 1988. Multiple sequence alignment with hierarchical clustering. *Nucleic Acids Res,* 16**,** 10881-90.

FILL, L., HADNEY, L., GRAVEN, K., PERSAUD, R. & HOSTOFFER, R. 2020. The clinical observation of a patient with common variable immunodeficiency diagnosed as having coronavirus disease 2019. *Ann Allergy Asthma Immunol,* 125**,** 112-114.

FU, Y., HAN, P., ZHU, R., BAI, T., YI, J., ZHAO, X., TAO, M., QUAN, R., CHEN, C., ZHANG, Y., HE, Q., JING, M., XIONG, X., TIAN, D. & YAN, W. 2020. Risk factors for viral RNA shedding in COVID-19 patients. *Eur Respir J,* 56.

FURSTENAU, M., LANGERBEINS, P., DE SILVA, N., FINK, A. M., ROBRECHT, S., VON TRESCKOW, J., SIMON, F., HOHLOCH, K., DROOGENDIJK, J., VAN DER KLIFT, M., VAN DER SPEK, E., ILLMER, T., SCHOTTKER, B., FISCHER, K., WENDTNER, C. M., TAUSCH, E., STILGENBAUER, S., NIEMANN, C. U., GREGOR, M., KATER, A. P., HALLEK, M. & EICHHORST, B. 2020. COVID-19 among fit patients with CLL treated with venetoclax-based combinations. *Leukemia,* 34**,** 2225-2229.

GORDON, A. *FASTX -Toolkit* [Online]. Available: http://hannonlab.cshl.edu/fastx_toolkit/ [Accessed].

GORDON, A. 2018. *"FASTX-Toolkit"* [Online]. Institute, B. Available: http://hannonlab.cshl.edu/fastx_toolkit/ [Accessed].

GUINDON, S., DUFAYARD, J. F., LEFORT, V., ANISIMOVA, M., HORDIJK, W. & GASCUEL, O. 2010. New algorithms and methods to estimate maximum-likelihood phylogenies: assessing the performance of PhyML 3.0. *Syst Biol,* 59**,** 307-21.

HADFIELD, J., MEGILL, C., BELL, S. M., HUDDLESTON, J., POTTER, B., CALLENDER, C., SAGULENKO, P., BEDFORD, T. & NEHER, R. A. 2018. Nextstrain: real-time tracking of pathogen evolution. *Bioinformatics,* 34**,** 4121-4123.

HARCOURT, J., TAMIN, A., LU, X., KAMILI, S., SAKTHIVEL, S. K., MURRAY, J., QUEEN, K., TAO, Y., PADEN, C. R., ZHANG, J., LI, Y., UEHARA, A., WANG, H., GOLDSMITH, C., BULLOCK, H. A., WANG, L., WHITAKER, B., LYNCH, B., GAUTAM, R., SCHINDEWOLF, C., LOKUGAMAGE, K. G., SCHARTON, D., PLANTE, J. A., MIRCHANDANI, D., WIDEN, S. G., NARAYANAN, K., MAKINO, S., KSIAZEK, T. G., PLANTE, K. S., WEAVER, S. C., LINDSTROM, S., TONG, S., MENACHERY, V. D. & THORNBURG, N. J. 2020. Severe Acute Respiratory Syndrome Coronavirus 2 from Patient with Coronavirus Disease, United States. *Emerg Infect Dis,* 26**,** 1266-1273.

HE, W., CHEN, L., CHEN, L., YUAN, G., FANG, Y., CHEN, W., WU, D., LIANG, B., LU, X., MA, Y., LI, L., WANG, H., CHEN, Z., LI, Q. & GALE, R. P. 2020a. COVID-19 in persons with haematological cancers. *Leukemia,* 34**,** 1637-1645.

HE, X., LAU, E. H. Y., WU, P., DENG, X., WANG, J., HAO, X., LAU, Y. C., WONG, J. Y., GUAN, Y., TAN, X., MO, X., CHEN, Y., LIAO, B., CHEN, W., HU, F., ZHANG, Q., ZHONG, M., WU, Y., ZHAO, L., ZHANG, F., COWLING, B. J., LI, F. & LEUNG, G. M. 2020b. Temporal dynamics in viral shedding and transmissibility of COVID-19. *Nat Med,* 26**,** 672-675.

HOANG, D. T., CHERNOMOR, O., VON HAESELER, A., MINH, B. Q. & VINH, L. S. 2018. UFBoot2: Improving the Ultrafast Bootstrap Approximation. *Mol Biol Evol,* 35**,** 518-522.

HU, Z., SONG, C., XU, C., JIN, G., CHEN, Y., XU, X., MA, H., CHEN, W., LIN, Y., ZHENG, Y., WANG, J., HU, Z., YI, Y. & SHEN, H. 2020. Clinical characteristics of 24 asymptomatic infections with COVID-19 screened among close contacts in Nanjing, China. *Sci China Life Sci,* 63**,** 706-711.

IKEGAMI, S., BENIRSCHKE, R., FLANAGAN, T., TANNA, N., KLEIN, T., ELUE, R., DEBOSZ, P., MALLEK, J., WRIGHT, G., GUARIGLIA, P., KANG, J. & GNIADEK, T. J. 2020. Persistence of SARS-CoV-2 nasopharyngeal swab PCR positivity in COVID-19 convalescent plasma donors. *Transfusion*.

INSTITUTE, B. 2018. *"Picard Toolkit"* [Online]. Broad Institute. Available: http://broadinstitute.github.io/picard [Accessed].

JARY, A., LEDUCQ, V., MALET, I., MAROT, S., KLEMENT-FRUTOS, E., TEYSSOU, E., SOULIE, C., ABDI, B., WIRDEN, M., POURCHER, V., CAUMES, E., CALVEZ, V., BURREL, S., MARCELIN, A. G. & BOUTOLLEAU, D. 2020. Evolution of viral quasispecies during SARS-CoV-2 infection. *Clin Microbiol Infect*.

JIN, X. H., ZHENG, K. I., PAN, K. H., XIE, Y. P. & ZHENG, M. H. 2020. COVID-19 in a patient with chronic lymphocytic leukaemia. *Lancet Haematol,* 7**,** e351-e352.

JUDSON, S. D. & MUNSTER, V. J. 2020. A framework for nosocomial transmission of emerging coronaviruses. *Infect Control Hosp Epidemiol***,** 1-2.

911 KALYAANAMOORTHY, S., MINH, B. Q., WONG, T. K. F., VON HAESELER, A. & JERMIIN, L. S. 2017.
912 ModelFinder: fast model selection for accurate phylogenetic estimates. *Nat Methods,* 14**,** 587-
913 589.
914 KATOH, K., MISAWA, K., KUMA, K. & MIYATA, T. 2002. MAFFT: a novel method for rapid multiple
915 sequence alignment based on fast Fourier transform. *Nucleic Acids Res,* 30**,** 3059-66.
916 KATOH, K. & STANDLEY, D. M. 2013. MAFFT multiple sequence alignment software version 7:
917 improvements in performance and usability. *Mol Biol Evol,* 30**,** 772-80.
918 KIM, D., LEE, J. Y., YANG, J. S., KIM, J. W., KIM, V. N. & CHANG, H. 2020. The Architecture of SARS-CoV-2
919 Transcriptome. *Cell,* 181**,** 914-921 e10.
920 KIM, S. H., KO, J. H., PARK, G. E., CHO, S. Y., HA, Y. E., KANG, J. M., KIM, Y. J., HUH, H. J., KI, C. S., JEONG,
921 B. H., PARK, J., JANG, J. H., KIM, W. S., KANG, C. I., CHUNG, D. R., SONG, J. H. & PECK, K. R. 2017.
922 Atypical presentations of MERS-CoV infection in immunocompromised hosts. *J Infect*
923 *Chemother,* 23**,** 769-773.
924 KUNISAKI, K. M. & JANOFF, E. N. 2009. Influenza in immunosuppressed populations: a review of
925 infection frequency, morbidity, mortality, and vaccine responses. *Lancet Infectious Diseases,* 9**,**
926 493-504.
927 LAN, L., XU, D., YE, G., XIA, C., WANG, S., LI, Y. & XU, H. 2020. Positive RT-PCR Test Results in Patients
928 Recovered From COVID-19. *JAMA*.
929 LANGMEAD, B. & SALZBERG, S. L. 2012. Fast gapped-read alignment with Bowtie 2. *Nat Methods,* 9**,** 357-
930 9.
931 LAU, S. Y., WANG, P., MOK, B. W., ZHANG, A. J., CHU, H., LEE, A. C., DENG, S., CHEN, P., CHAN, K. H.,
932 SONG, W., CHEN, Z., TO, K. K., CHAN, J. F., YUEN, K. Y. & CHEN, H. 2020. Attenuated SARS-CoV-2
933 variants with deletions at the S1/S2 junction. *Emerg Microbes Infect,* 9**,** 837-842.
934 LEE, S., KIM, T., LEE, E., LEE, C., KIM, H., RHEE, H., PARK, S. Y., SON, H. J., YU, S., PARK, J. W., CHOO, E. J.,
935 PARK, S., LOEB, M. & KIM, T. H. 2020. Clinical Course and Molecular Viral Shedding Among
936 Asymptomatic and Symptomatic Patients With SARS-CoV-2 Infection in a Community Treatment
937 Center in the Republic of Korea. *JAMA Intern Med*.
938 LI, H., HANDSAKER, B., WYSOKER, A., FENNELL, T., RUAN, J., HOMER, N., MARTH, G., ABECASIS, G.,
939 DURBIN, R. & GENOME PROJECT DATA PROCESSING, S. 2009. The Sequence Alignment/Map
940 format and SAMtools. *Bioinformatics,* 25**,** 2078-9.
941 LI, J., ZHANG, L., LIU, B. & SONG, D. 2020. Case Report: Viral Shedding for 60 Days in a Woman with
942 COVID-19. *Am J Trop Med Hyg,* 102**,** 1210-1213.
943 LIU, L., WANG, P., NAIR, M. S., YU, J., RAPP, M., WANG, Q., LUO, Y., CHAN, J. F., SAHI, V., FIGUEROA, A.,
944 GUO, X. V., CERUTTI, G., BIMELA, J., GORMAN, J., ZHOU, T., CHEN, Z., YUEN, K. Y., KWONG, P. D.,
945 SODROSKI, J. G., YIN, M. T., SHENG, Z., HUANG, Y., SHAPIRO, L. & HO, D. D. 2020a. Potent
946 Neutralizing Monoclonal Antibodies Directed to Multiple Epitopes on the SARS-CoV-2 Spike.
947 *bioRxiv*.
948 LIU, W. D., CHANG, S. Y., WANG, J. T., TSAI, M. J., HUNG, C. C., HSU, C. L. & CHANG, S. C. 2020b.
949 Prolonged virus shedding even after seroconversion in a patient with COVID-19. *J Infect,* 81**,** 318-
950 356.
951 LIU, Y., CHEN, X., ZOU, X. & LUO, H. 2020c. A severe-type COVID-19 case with prolonged virus shedding. *J*
952 *Formos Med Assoc*.
953 LIU, Z., ZHENG, H., LIN, H., LI, M., YUAN, R., PENG, J., XIONG, Q., SUN, J., LI, B., WU, J., YI, L., PENG, X.,
954 ZHANG, H., ZHANG, W., HULSWIT, R. J. G., LOMAN, N., RAMBAUT, A., KE, C., BOWDEN, T. A.,
955 PYBUS, O. G. & LU, J. 2020d. Identification of common deletions in the spike protein of SARS-
956 CoV-2. *J Virol*.
957 LONG, Q. X., TANG, X. J., SHI, Q. L., LI, Q., DENG, H. J., YUAN, J., HU, J. L., XU, W., ZHANG, Y., LV, F. J., SU,
958 K., ZHANG, F., GONG, J., WU, B., LIU, X. M., LI, J. J., QIU, J. F., CHEN, J. & HUANG, A. L. 2020.

Clinical and immunological assessment of asymptomatic SARS-CoV-2 infections. *Nat Med,* 26**,** 1200-1204.

MARTIN, M. 2011. Cutadapt removes adapter sequences from high-throughput sequencing reads. *EMBnet.journal,* 17**,** 10-12.

MCKENNA, A., HANNA, M., BANKS, E., SIVACHENKO, A., CIBULSKIS, K., KERNYTSKY, A., GARIMELLA, K., ALTSHULER, D., GABRIEL, S., DALY, M. & DEPRISTO, M. A. 2010. The Genome Analysis Toolkit: a MapReduce framework for analyzing next-generation DNA sequencing data. *Genome Res,* 20**,** 1297-303.

MCMICHAEL, T. M., CLARK, S., POGOSJANS, S., KAY, M., LEWIS, J., BAER, A., KAWAKAMI, V., LUKOFF, M. D., FERRO, J., BROSTROM-SMITH, C., RIEDO, F. X., RUSSELL, D., HIATT, B., MONTGOMERY, P., RAO, A. K., CURRIE, D. W., CHOW, E. J., TOBOLOWSKY, F., BARDOSSY, A. C., OAKLEY, L. P., JACOBS, J. R., SCHWARTZ, N. G., STONE, N., REDDY, S. C., JERNIGAN, J. A., HONEIN, M. A., CLARK, T. A., DUCHIN, J. S., PUBLIC HEALTH, S., KING COUNTY, E. & TEAM, C. C.-I. 2020a. COVID-19 in a Long-Term Care Facility - King County, Washington, February 27-March 9, 2020. *MMWR Morb Mortal Wkly Rep,* 69**,** 339-342.

MCMICHAEL, T. M., CURRIE, D. W., CLARK, S., POGOSJANS, S., KAY, M., SCHWARTZ, N. G., LEWIS, J., BAER, A., KAWAKAMI, V., LUKOFF, M. D., FERRO, J., BROSTROM-SMITH, C., REA, T. D., SAYRE, M. R., RIEDO, F. X., RUSSELL, D., HIATT, B., MONTGOMERY, P., RAO, A. K., CHOW, E. J., TOBOLOWSKY, F., HUGHES, M. J., BARDOSSY, A. C., OAKLEY, L. P., JACOBS, J. R., STONE, N. D., REDDY, S. C., JERNIGAN, J. A., HONEIN, M. A., CLARK, T. A., DUCHIN, J. S., PUBLIC, H.-S., KING COUNTY, E. & TEAM, C. C.-I. 2020b. Epidemiology of Covid-19 in a Long-Term Care Facility in King County, Washington. *N Engl J Med,* 382**,** 2005-2011.

MIRA, E., YARCE, O. A., ORTEGA, C., FERNANDEZ, S., PASCUAL, N. M., GOMEZ, C., ALVAREZ, M. A., MOLINA, I. J., LAMA, R. & SANTAMARIA, M. 2020. Rapid recovery of a SARS-CoV-2-infected X-linked agammaglobulinemia patient after infusion of COVID-19 convalescent plasma. *J Allergy Clin Immunol Pract*.

NGUYEN, L. T., SCHMIDT, H. A., VON HAESELER, A. & MINH, B. Q. 2015. IQ-TREE: a fast and effective stochastic algorithm for estimating maximum-likelihood phylogenies. *Mol Biol Evol,* 32**,** 268-74.

PANEESHA, S., PRATT, G., PARRY, H. & MOSS, P. 2020. Covid-19 infection in therapy-naive patients with B-cell chronic lymphocytic leukemia. *Leuk Res,* 93**,** 106366.

PRESCOTT, J., FALZARANO, D., DE WIT, E., HARDCASTLE, K., FELDMANN, F., HADDOCK, E., SCOTT, D., FELDMANN, H. & MUNSTER, V. J. 2018. Pathogenicity and Viral Shedding of MERS-CoV in Immunocompromised Rhesus Macaques. *Front Immunol,* 9**,** 205.

QIAN, G. Q., CHEN, X. Q., LV, D. F., MA, A. H. Y., WANG, L. P., YANG, N. B. & CHEN, X. M. 2020. Duration of SARS-CoV-2 viral shedding during COVID-19 infection. *Infect Dis (Lond),* 52**,** 511-512.

RAMBAUT, A., HOLMES, E. C., O'TOOLE, A., HILL, V., MCCRONE, J. T., RUIS, C., DU PLESSIS, L. & PYBUS, O. G. 2020. A dynamic nomenclature proposal for SARS-CoV-2 lineages to assist genomic epidemiology. *Nat Microbiol*.

ROBERT, X. & GOUET, P. 2014. Deciphering key features in protein structures with the new ENDscript server. *Nucleic Acids Res,* 42**,** W320-4.

ROBINSON, J. T., THORVALDSDOTTIR, H., WENGER, A. M., ZEHIR, A. & MESIROV, J. P. 2017. Variant Review with the Integrative Genomics Viewer. *Cancer Res,* 77**,** e31-e34.

SAGULENKO, P., PULLER, V. & NEHER, R. A. 2018. TreeTime: Maximum-likelihood phylodynamic analysis. *Virus Evol,* 4**,** vex042.

SALAZAR, E., PEREZ, K. K., ASHRAF, M., CHEN, J., CASTILLO, B., CHRISTENSEN, P. A., EUBANK, T., BERNARD, D. W., EAGAR, T. N., LONG, S. W., SUBEDI, S., OLSEN, R. J., LEVEQUE, C., SCHWARTZ, M. R., DEY, M., CHAVEZ-EAST, C., ROGERS, J., SHEHABELDIN, A., JOSEPH, D., WILLIAMS, G., THOMAS, K., MASUD, F., TALLEY, C., DLOUHY, K. G., LOPEZ, B. V., HAMPTON, C., LAVINDER, J.,

GOLLIHAR, J. D., MARANHAO, A. C., IPPOLITO, G. C., SAAVEDRA, M. O., CANTU, C. C., YERRAMILLI, P., PRUITT, L. & MUSSER, J. M. 2020. Treatment of Coronavirus Disease 2019 (COVID-19) Patients with Convalescent Plasma. *Am J Pathol,* 190**,** 1680-1690.

SCHUBERT, M., LINDGREEN, S. & ORLANDO, L. 2016. AdapterRemoval v2: rapid adapter trimming, identification, and read merging. *BMC Res Notes,* 9**,** 88.

SHEN, Z., XIAO, Y., KANG, L., MA, W., SHI, L., ZHANG, L., ZHOU, Z., YANG, J., ZHONG, J., YANG, D., GUO, L., ZHANG, G., LI, H., XU, Y., CHEN, M., GAO, Z., WANG, J., REN, L. & LI, M. 2020. Genomic Diversity of Severe Acute Respiratory Syndrome-Coronavirus 2 in Patients With Coronavirus Disease 2019. *Clin Infect Dis,* 71**,** 713-720.

SHU, Y. & MCCAULEY, J. 2017. GISAID: Global initiative on sharing all influenza data - from vision to reality. *Euro Surveill,* 22.

SORESINA, A., MORATTO, D., CHIARINI, M., PAOLILLO, C., BARESI, G., FOCA, E., BEZZI, M., BARONIO, B., GIACOMELLI, M. & BADOLATO, R. 2020. Two X-linked agammaglobulinemia patients develop pneumonia as COVID-19 manifestation but recover. *Pediatr Allergy Immunol*.

SPERANZA, E., WILLIAMSON, B. N., FELDMANN, F., STURDEVANT, G. L., PEREZ-PEREZ, L., MEAD-WHITE, K., SMITH, B. J., LOVAGLIO, J., MARTENS, C., MUNSTER, V. J., OKUMURA, A., SHAIA, C., FELDMANN, H., BEST, S. M. & DE WIT, E. 2020. SARS-CoV-2 infection dynamics in lungs of African green monkeys. *bioRxiv*.

SUN, J., XIAO, J., SUN, R., TANG, X., LIANG, C., LIN, H., ZENG, L., HU, J., YUAN, R., ZHOU, P., PENG, J., XIONG, Q., CUI, F., LIU, Z., LU, J., TIAN, J., MA, W. & KE, C. 2020. Prolonged Persistence of SARS-CoV-2 RNA in Body Fluids. *Emerg Infect Dis,* 26**,** 1834-1838.

VAN DER VRIES, E., STITTELAAR, K. J., VAN AMERONGEN, G., VELDHUIS KROEZE, E. J., DE WAAL, L., FRAAIJ, P. L., MEESTERS, R. J., LUIDER, T. M., VAN DER NAGEL, B., KOCH, B., VULTO, A. G., SCHUTTEN, M. & OSTERHAUS, A. D. 2013. Prolonged influenza virus shedding and emergence of antiviral resistance in immunocompromised patients and ferrets. *PLoS Pathog,* 9**,** e1003343.

VAN KAMPEN, J. J. A., VAN DE VIJVER, D. A. M. C., FRAAIJ, P. L. A., HAAGMANS, B. L., LAMERS, M. M., OKBA, N., VAN DEN AKKER, J. P. C., ENDEMAN, H., GOMMERS, D. A. M. P. J., CORNELISSEN, J. J., HOEK, R. A. S., VAN DER EERDEN, M. M., HESSELINK, D. A., METSELAAR, H. J., VERBON, A., DE STEENWINKEL, J. E. M., ARON, G. I., VAN GORP, E. C. M., VAN BOHEEMEN, S., VOERMANS, J. C., BOUCHER, C. A. B., MOLENKAMP, R., KOOPMANS, M. P. G., GEURTSVANKESSEL, C. & VAN DER EIJK, A. A. 2020. Shedding of infectious virus in hospitalized patients with coronavirus disease-2019 (COVID-19): duration and key determinants. *medRxiv***,** 2020.06.08.20125310.

WALLS, A. C., PARK, Y. J., TORTORICI, M. A., WALL, A., MCGUIRE, A. T. & VEESLER, D. 2020. Structure, Function, and Antigenicity of the SARS-CoV-2 Spike Glycoprotein. *Cell,* 181**,** 281-292 e6.

WANG, W., XU, Y., GAO, R., LU, R., HAN, K., WU, G. & TAN, W. 2020. Detection of SARS-CoV-2 in Different Types of Clinical Specimens. *JAMA*.

WANG Y., G. M., PERLMAN S. 2020. Coronaviruses: An Updated Overview of Their Replication and Pathogenesis. *In:* MAIER H., B. E. (ed.) *Coronaviruses. Methods in Molecular Biology.* NY: Humana, New York, NY.

WOLFEL, R., CORMAN, V. M., GUGGEMOS, W., SEILMAIER, M., ZANGE, S., MULLER, M. A., NIEMEYER, D., JONES, T. C., VOLLMAR, P., ROTHE, C., HOELSCHER, M., BLEICKER, T., BRUNINK, S., SCHNEIDER, J., EHMANN, R., ZWIRGLMAIER, K., DROSTEN, C. & WENDTNER, C. 2020. Virological assessment of hospitalized patients with COVID-2019. *Nature,* 581**,** 465-469.

WRAPP, D., WANG, N., CORBETT, K. S., GOLDSMITH, J. A., HSIEH, C. L., ABIONA, O., GRAHAM, B. S. & MCLELLAN, J. S. 2020. Cryo-EM structure of the 2019-nCoV spike in the prefusion conformation. *Science,* 367**,** 1260-1263.

1053 WROBEL, A. G., BENTON, D. J., XU, P., ROUSTAN, C., MARTIN, S. R., ROSENTHAL, P. B., SKEHEL, J. J. &
1054 GAMBLIN, S. J. 2020. SARS-CoV-2 and bat RaTG13 spike glycoprotein structures inform on virus
1055 evolution and furin-cleavage effects. *Nat Struct Mol Biol*.
1056 ZHU, L., XU, X., MA, K., YANG, J., GUAN, H., CHEN, S., CHEN, Z. & CHEN, G. 2020. Successful recovery of
1057 COVID-19 pneumonia in a renal transplant recipient with long-term immunosuppression. *Am J*
1058 *Transplant,* 20**,** 1859-1863.
1059 ZOU, L., RUAN, F., HUANG, M., LIANG, L., HUANG, H., HONG, Z., YU, J., KANG, M., SONG, Y., XIA, J., GUO,
1060 Q., SONG, T., HE, J., YEN, H. L., PEIRIS, M. & WU, J. 2020. SARS-CoV-2 Viral Load in Upper
1061 Respiratory Specimens of Infected Patients. *N Engl J Med,* 382**,** 1177-1179.

1062

In Brief:

This case study describes a female immunocompromised patient with chronic lymphocytic leukemia and acquired hypogammaglobulinemia who became persistently infected with SARS-CoV-2. Though asymptomatic throughout the course of infection, the patient demonstrated prolonged shedding of both infectious SARS-CoV-2 virus and RNA. This study demonstrates certain patients may remain infectious for prolonged periods of time and highlights the need for further studies to understand risk factors for prolonged infectious SARS-CoV-2 shedding.

Highlights:

- Persistent SARS-CoV-2 infection and shedding in immunocompromised patient
- Infectious SARS-CoV-2 isolated up to 70 days post diagnosis
- Observed within-host genetic variation with continuous turnover of viral variants
- Patient SARS-CoV-2 isolates do not display altered replication

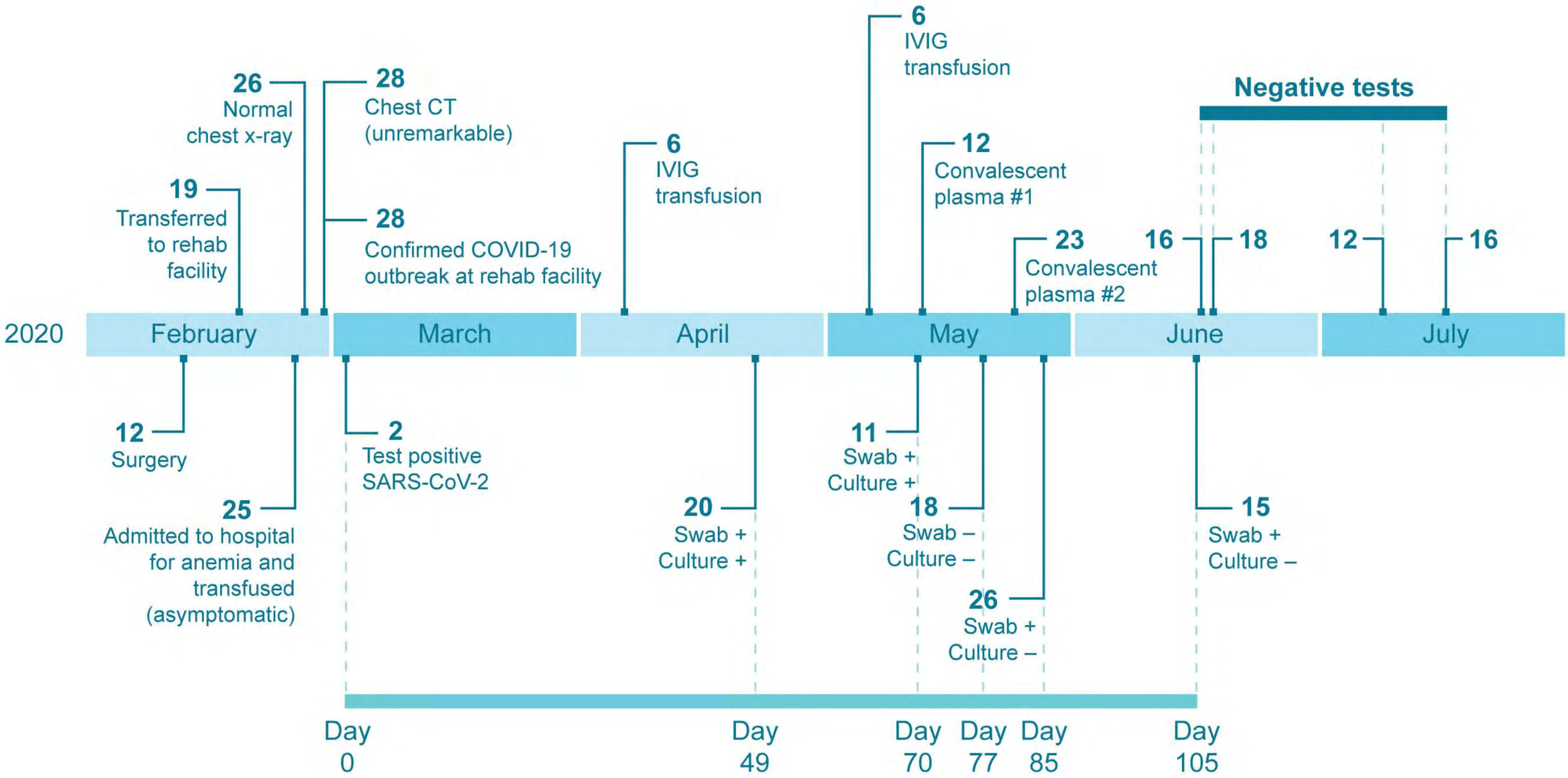
2020
February
March
April
May
June
July
26
Normal chest x-ray
28
Chest CT (unremarkable)
19
Transferred to rehab facility
28
Confirmed COVID-19 outbreak at rehab facility
6
IVIG transfusion
6
IVIG transfusion
12
Convalescent plasma #1
23
Convalescent plasma #2
Negative tests
16
18
12
16
12
Surgery
25
Admitted to hospital for anemia and transfused (asymptomatic)
2
Test positive SARS-CoV-2
20
Swab +
Culture +
11
Swab +
Culture +
18
Swab –
Culture –
26
Swab +
Culture –
15
Swab +
Culture –
Day 0
Day 49
Day 70
Day 77
Day 85
Day 105

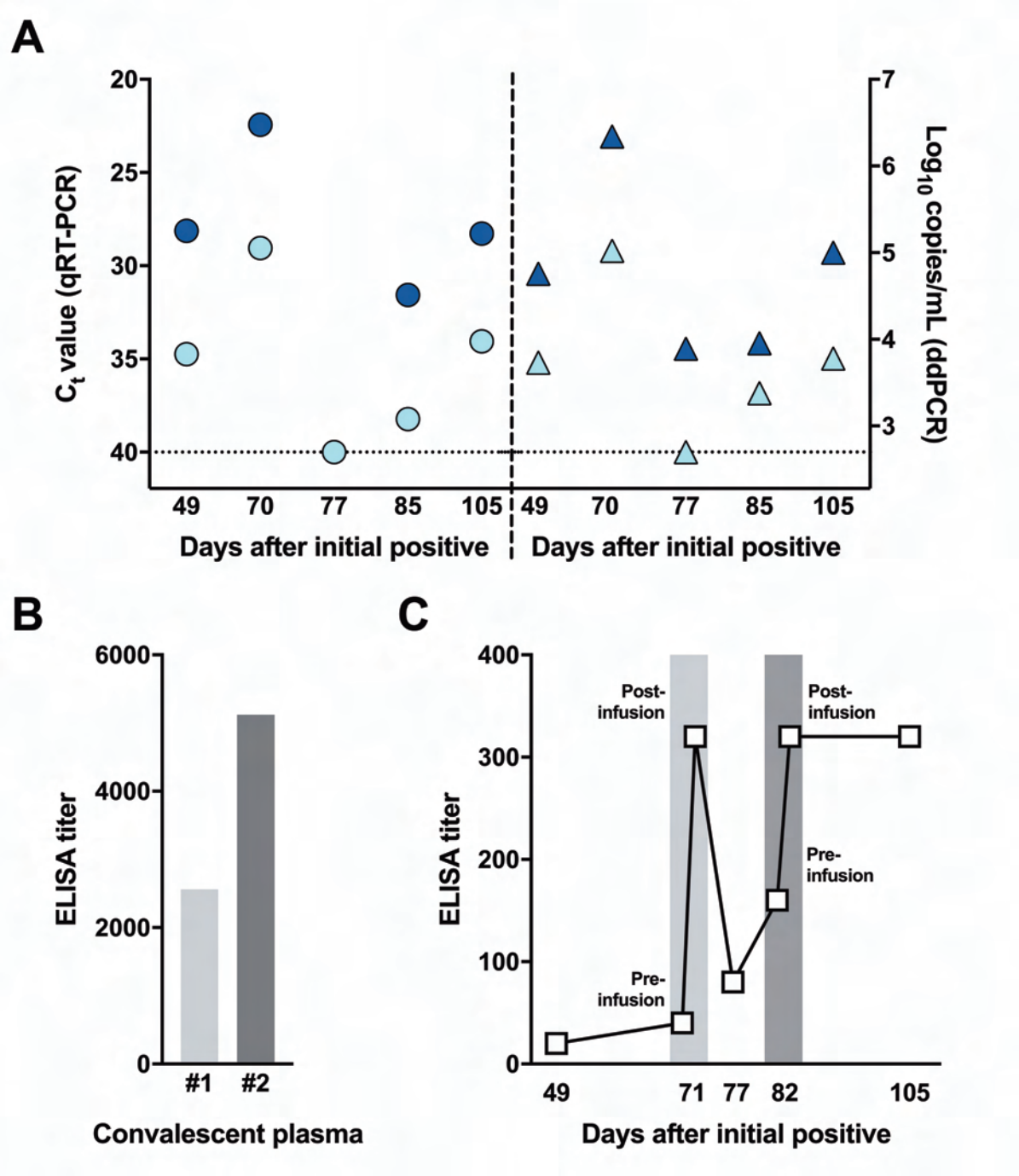
A
20
25
30
35
40
C_t value (qRT-PCR)
7
6
5
4
3
Log_{10} copies/mL (ddPCR)
49
70
77
85
105
Days after initial positive
Days after initial positive
B
6000
4000
2000
0
ELISA titer
#1
#2
Convalescent plasma
C
400
300
200
100
0
ELISA titer
Post-infusion
Post-infusion
Pre-infusion
Pre-infusion
49
71
77
82
105
Days after initial positive

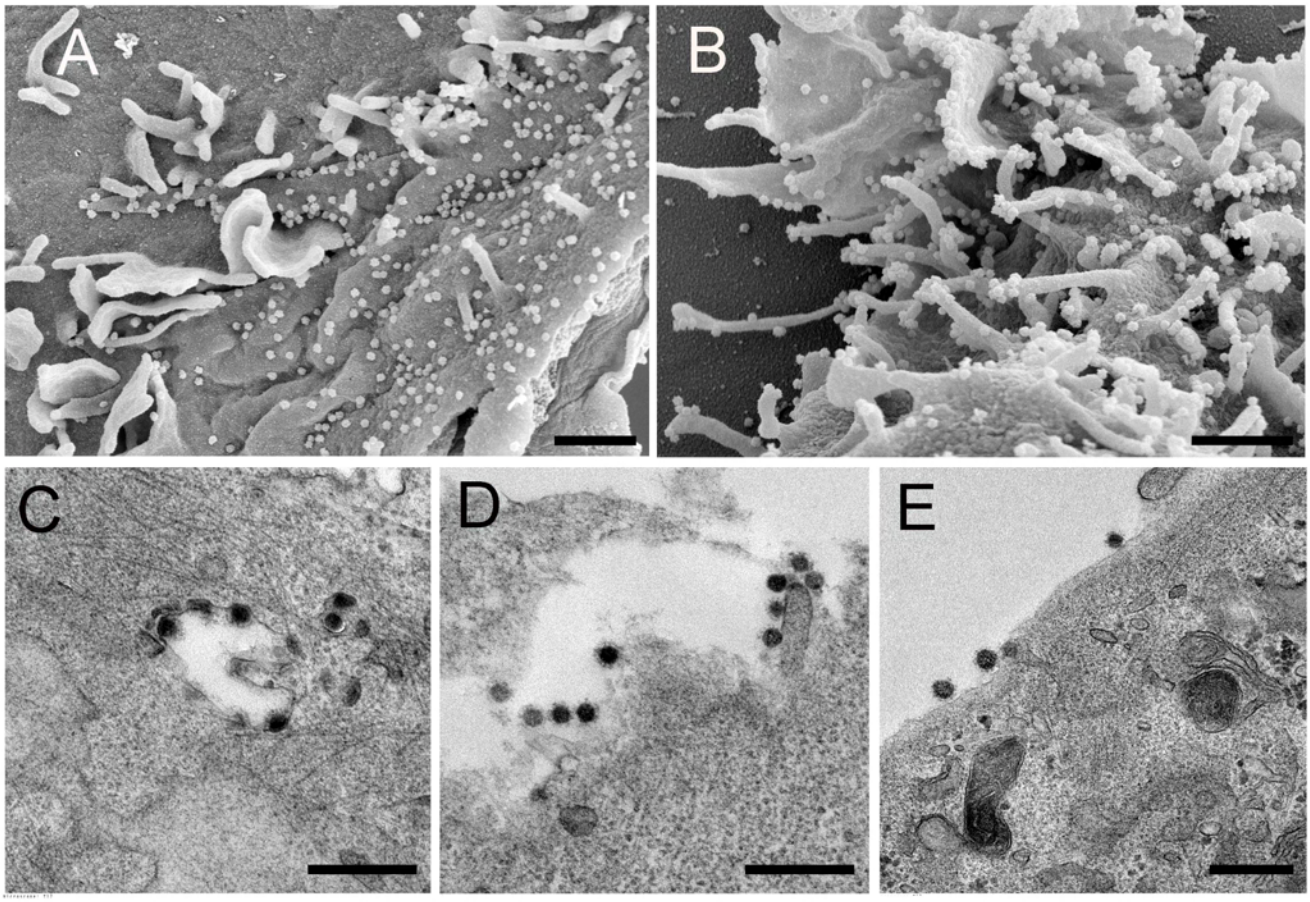
A
B
C
D
E

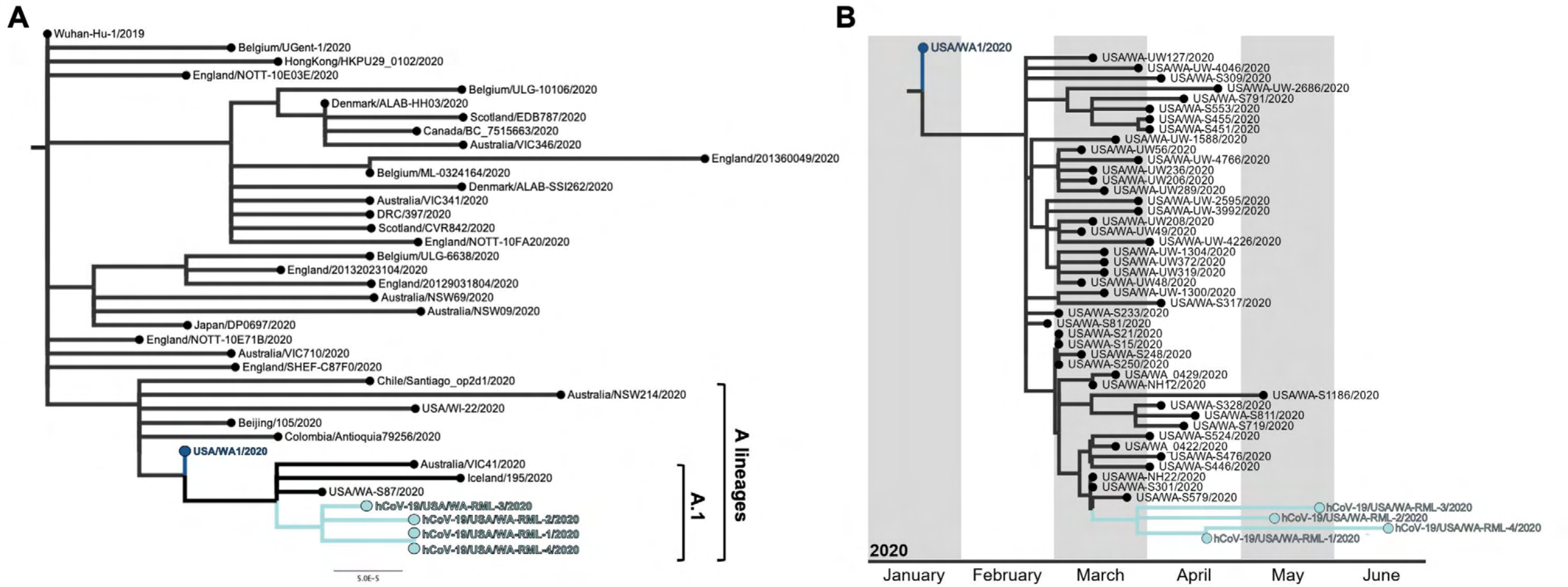
A
Wuhan-Hu-1/2019
Belgium/UGent-1/2020
HongKong/HKPU29_0102/2020
England/NOTT-10E03E/2020
Belgium/ULG-10106/2020
Denmark/ALAB-HH03/2020
Scotland/EDB787/2020
Canada/BC_7515663/2020
Australia/VIC346/2020
England/201360049/2020
Belgium/ML-0324164/2020
Denmark/ALAB-SSI262/2020
Australia/VIC341/2020
DRC/397/2020
Scotland/CVR842/2020
England/NOTT-10FA20/2020
Belgium/ULG-6638/2020
England/20132023104/2020
England/20129031804/2020
Australia/NSW69/2020
Australia/NSW09/2020
Japan/DP0697/2020
England/NOTT-10E71B/2020
Australia/VIC710/2020
England/SHEF-C87F0/2020
Chile/Santiago_op2d1/2020
Australia/NSW214/2020
USA/WI-22/2020
Beijing/105/2020
Colombia/Antioquia79256/2020
USA/WA1/2020
Australia/VIC41/2020
Iceland/195/2020
USA/WA-S87/2020
hCoV-19/USA/WA-RML-3/2020
hCoV-19/USA/WA-RML-2/2020
hCoV-19/USA/WA-RML-1/2020
hCoV-19/USA/WA-RML-4/2020
A lineages
A.1
5.0E-5
B
USA/WA1/2020
USA/WA-UW127/2020
USA/WA-UW-4046/2020
USA/WA-S309/2020
USA/WA-UW-2686/2020
USA/WA-S791/2020
USA/WA-S553/2020
USA/WA-S455/2020
USA/WA-S451/2020
USA/WA-UW-1588/2020
USA/WA-UW56/2020
USA/WA-UW-4766/2020
USA/WA-UW236/2020
USA/WA-UW206/2020
USA/WA-UW289/2020
USA/WA-UW-2595/2020
USA/WA-UW-3992/2020
USA/WA-UW208/2020
USA/WA-UW49/2020
USA/WA-UW-4226/2020
USA/WA-UW-1304/2020
USA/WA-UW372/2020
USA/WA-UW319/2020
USA/WA-UW48/2020
USA/WA-UW-1300/2020
USA/WA-S317/2020
USA/WA-S233/2020
USA/WA-S81/2020
USA/WA-S21/2020
USA/WA-S15/2020
USA/WA-S248/2020
USA/WA-S250/2020
USA/WA_0429/2020
USA/WA-NH12/2020
USA/WA-S1186/2020
USA/WA-S328/2020
USA/WA-S811/2020
USA/WA-S719/2020
USA/WA-S524/2020
USA/WA_0422/2020
USA/WA-S476/2020
USA/WA-S446/2020
USA/WA-NH22/2020
USA/WA-S301/2020
USA/WA-S579/2020
hCoV-19/USA/WA-RML-3/2020
hCoV-19/USA/WA-RML-2/2020
hCoV-19/USA/WA-RML-4/2020
hCoV-19/USA/WA-RML-1/2020
2020
January
February
March
April
May
June

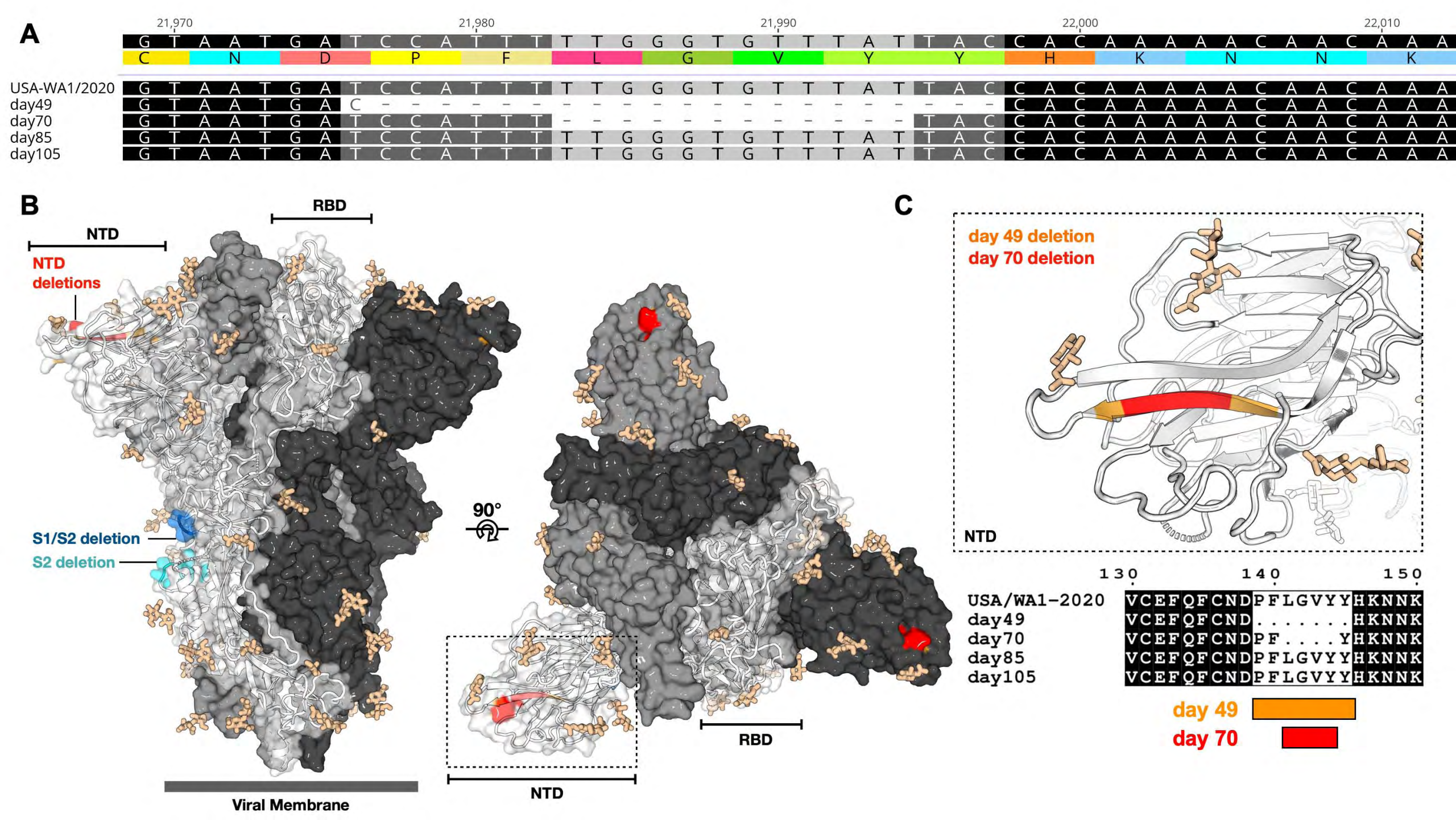
A
21,970
21,980
21,990
22,000
22,010
G T A A T G A T C C A T T T T T G G G T G T T T A T T A C C A C A A A A A A C A A C A A A
C N D P F L G V Y Y H K N N K
USA-WA1/2020
day49
day70
day85
day105
B
NTD
RBD
NTD deletions
S1/S2 deletion
S2 deletion
90°
Viral Membrane
RBD
NTD
C
day 49 deletion
day 70 deletion
NTD
130
140
150
USA/WA1-2020 VCEFQFCNDPFLGVYYHKNNK
day49 VCEFQFCND.....HKNNK
day70 VCEFQFCNDPF....YHKNNK
day85 VCEFQFCNDPFLGVYYHKNNK
day105 VCEFQFCNDPFLGVYYHKNNK
day 49
day 70

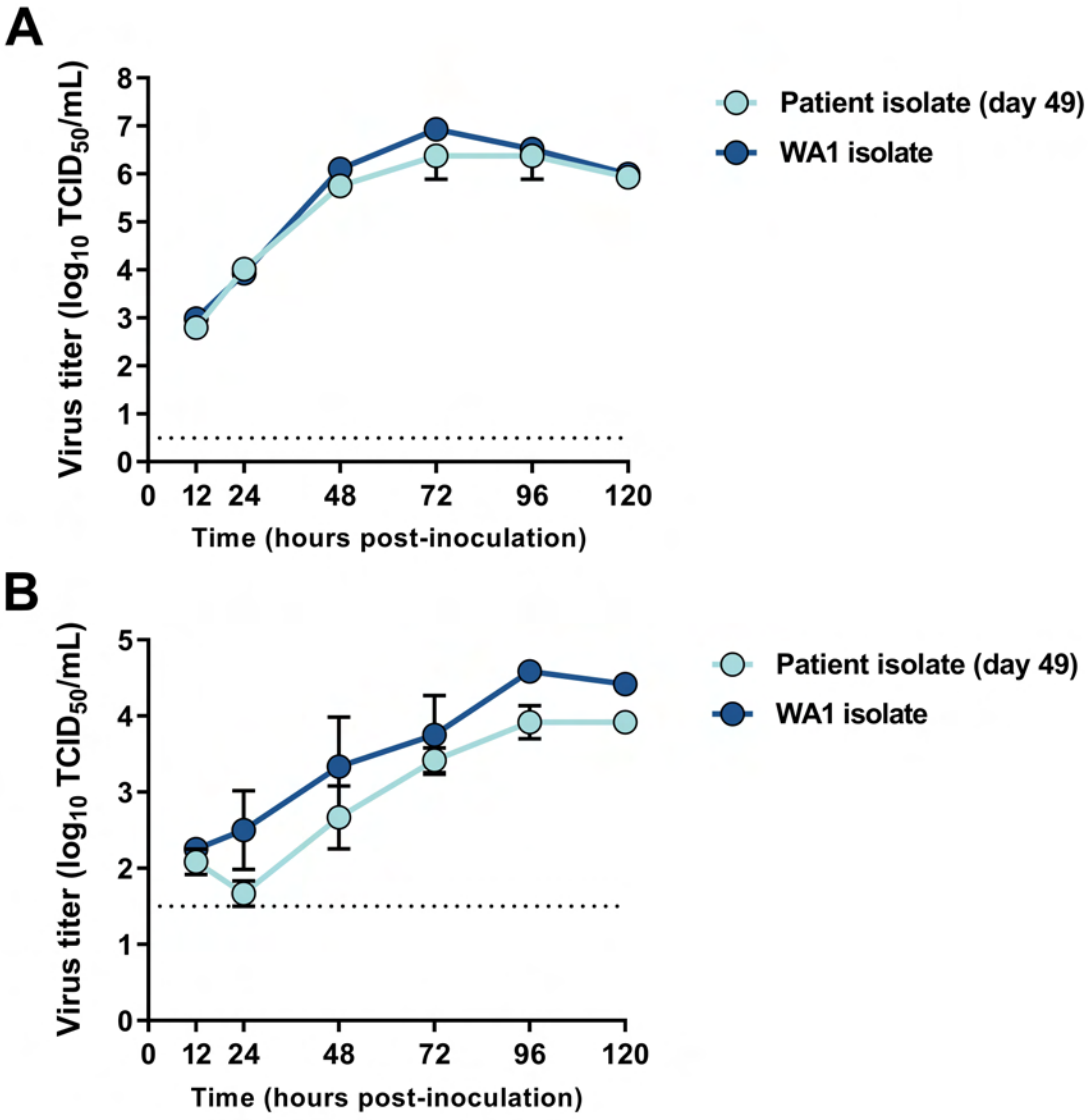
A
Virus titer (log10 TCID50/mL)
8
7
6
5
4
3
2
1
0
0
12
24
48
72
96
120
Time (hours post-inoculation)
Patient isolate (day 49)
WA1 isolate
B
Virus titer (log10 TCID50/mL)
5
4
3
2
1
0
0
12
24
48
72
96
120
Time (hours post-inoculation)
Patient isolate (day 49)
WA1 isolate